UNIVERSIDAD POLITÉCNICA DE VALENCIA

Instituto de Investigación e Innovación en Bioingeniería y Tecnologías Aplicadas al Ser Humano

UNIVERSITÀ DI BOLOGNA

Dipartimento di Elettronica, Informatica, Sistemistica

Simulating the Effects of Polyunsaturated Fatty Acids on Human Slowly Activating Delayed Rectifier Potassium Channel (KCNQ1 - KCNE1)

FINAL MASTER'S PROJECT

PRESENTED BY

Tomáš Starý

SUPERVISED BY

Dr. Stefano Severi

Dr. Sanjay Kharche

Dr. José María Ferrero De Loma-Osorio

Acknowledgements

I would like to show my gratitude to my supervisors. This work would not have been possible without their support and useful comments. I'm grateful to Stefano Severi for provide me place in his lab to develop this work. To José María Ferrero De Loma-Osorio whose classes awakened my interest to develop this work. I would like to express especial thanks to Sanjay Kharche who provided day to day supervision in this work and also supported code development, simulations, and manuscript writing.

I owe sincere and earnest thankfulness to Carmen Valenzuela and her collaborators who kindly provided experimental data and useful information.

I thank to the employees of International Exchange Programmes Office, administration of MSc in Biomedical Engineering and to the Erasmus programme who made available my stay in Italy. To the scholarship from Spanish Ministry of Education which supported me during my MSc degree studies.

Besides, I'm pleased to thank to my family and my friends who encourage me to keep going.

Abstract

The consumption of ω-3 polyunsaturated fatty acids (PUFA) from fish oil is recommended to prevent arrhythmias and reduce risk of sudden cardiac death. PUFA modulate activity of various cardiac ion channels.

The models of electrical activity of the heart based on mathematical formulation are a part of the efforts to improve the understanding and prediction of heart behaviour. The ion channels gating models are a basic part of models of cardiac electrical activity. The human slowly activated delayed rectifier potassium channel (I_{Ks}) is a key contributor to ventricle repolarization.

The goal of this study is to determine the effects of PUFA on I_{Ks}. Further it aims to predict the effects of PUFA induced alteration in I_{Ks} on the ventricular action potential (AP). Eicosapentaenoic acid (EPA) and docosahexaenoic acid (DHA) were used to perform the experiments.

The Markov chain formulation of ion channel models constitutes an important improvement and is able to adequately describe the kinetic behaviour of the channel. The I_{Ks} Markovian model involves 17 conformation states and 15 parameters. This model was used to simulate the data obtained from voltage clamp experiment. The parameters of the model were identified using Nelder-Mead simplex method.

The main results are the following. Acute exposure to PUFA increased I_{Ks} and augment the time constant. The Chronic exposure reduced I_{Ks}. Incorporating the identified model to human ventricle cell model caused AP prolongation in the Chronic case. The Acute EPA exposure caused AP shortening. The Acute DHA had no significant effect to AP in ten Tusscher et al. model and caused AP shortening in O'Hara et al. model. The Grandi et al. model was insensitive to I_{Ks} modifications.

In conclusion the underlying mechanism of PUFA is very complex. Effects on the I_{Ks} and AP is may have proarrhythmic as well as antiarrhythmic consequences. Thus, the advice to increase the intake of PUFA should be adjusted with respect to pathophysiological setting of individual patient.

Resumen

El consumo de ácidos grasos omega-3 poliinsaturados (PUFA) que se encuentran en general en los pescados, es recomendado para prevenir y disminuir el riesgo de muerte súbita. Se ha comprobado que los PUFA modifican la actividad de diversos canales iónicos del corazón.

Los modelos de la actividad eléctrica del corazón basado en la formulación matemática hacen parte de los esfuerzos realizados para mejorar la comprensión y predicción del comportamiento del corazón. Los modelos de los canales iónicos forman la base de los modelos de la actividad eléctrica cardíaca. Tal es el caso del canal humano de potasio rectificador retardado de activación lenta (I_{Ks}) que es un factor clave en la repolarización ventricular.

El objetivo de este estudio es determinar los efectos de los PUFA en los canales I_{Ks}. Además se pretende predecir los efectos inducidos de los PUFA en los I_{Ks} sobre el potencial de acción (PA) ventricular. En este estudio, el ácido eicosapentaenoico (EPA) y el ácido docosahexaenoico (DHA) se utilizaron para realizar diversos protocolos experimentales.

La cadena de Markov, constituye una mejora importante de los modelos de canales iónicos y es capaz de describir adecuadamente el comportamiento cinético del canal. El modelo de Markov del canal I_{Ks} incluye a 17 estados conformacionales y 15 parámetros. Este modelo fue utilizado para simular los datos obtenidos de los experimentos de voltage clamp. Los parámetros del modelo fueron identificados por el método de Nelder-Mead.

Los principales resultados obtenidos fueron los siguientes: La exposición aguda de los PUFA aumenta la corriente de I_{Ks} y la constante de tiempo. La exposición crónica reduce la I_{Ks}. La incorporación del modelo identificado del canal de I_{Ks} al modelo celular del ventrículo humano, causa prolongación de la duración del potencial de acción en el caso crónico. La exposición aguda de EPA causa acortamiento de la duración del potencial de acción en el modelo de O´Hara et al. El modelo de Grandi et al, fue insensible a las modificaciones de la I_{Ks}.

En conclusión, el mecanismo subyacente de ácidos grasos poliinsaturados es muy complejo. Los efectos sobre la I_{Ks} y la duración del potencial de acción pueden tener consecuencias proarrítmicas, así como antiarrítmicas. Por lo tanto, el consejo de aumentar la ingesta de PUFA debe ser ajustada con respecto a la situación fisiopatológica de cada paciente.

Abstrakt

Pro snížení rizika arytmií a náhlého srdečního úmrtí je doporučována konzumace ω-3 více nenasycených mastných kyselin (PUFA) obsažených v rybím tuku. PUFA mají vliv na činnost celé řady iontových kanálů vyskytujících se v lidském srdci.

Modelování elektrické srdeční aktivity na základě matematické formulace elektrofyziologické funkce srdce je součástí snahy o lepší pochopení a předvídání srdeční činnosti. Základem těchto modelů jsou modely iontových kanálů. Pomalu aktivovaný kanál draslíku I_{Ks} je klíčovým kanálem repolarizačního proudu v lidských srdečních komorách.

Cílem této studie je určit vliv PUFA na I_{Ks} a modelování účinků těchto změn na akční potenciál (AP) buněk srdečních komor. V této studii byl zkoumán vliv ekosapentaenové kyseliny (EPA) a dokosahexaenové kyseliny.

Modely založené na Markovově řetězci představují významný pokrok ve vysvětlení funkce iontových kanálů a jejich kinetických vlastností. Markovův model kanálu I_{Ks} zahrnuje 17 stavů a 15 parametrů, které popisují přechody mezi jednotlivými stavy. Tento model byl použit pro simulaci dat získaných z pokusů provedených metodou voltage clamp. Parametry modelů byly určeny pomocí algoritmu vynalezeného autory Nelder a Mead.

Výsledky této studie jsou následující. Akutní aplikace PUFA způsobuje zvýšení I_{Ks} a časové konstanty. Chronická aplikace má za důsledek snížení I_{Ks}. Implementace identifikovaného modelu I_{Ks} do modelu lidské komory způsobuje prodloužení AP při simulaci účinků chronické aplikace ve všech testovaných modelech. V případě účinků akutní aplikace EPA je důsledkem zkrácení AP. Akutní aplikace DHA nemá podle modelu ten Tuschera a kol. významný vliv na AP a způsobuje zkrácení AP podle modelu O'Hara a kol. Model Grandi a kol. není citlivý ke změnám velikosti I_{Ks}.

Účinky PUFA jsou velmi komplexním jevem. Vliv na I_{Ks} a AP může mít za důsledek jak potlačení arytmií tak jejich vyvolávání. Z tohoto důvodu je nutné přizpůsobit doporučení o příjmu PUFA s ohledem na individuální patofyziologický stav jednotlivých pacientů.

Index

Index of Figures

Index of Tables

1 Introduction

The human heart must beat 80 times a minute. With every contraction the blood is pumped into the body in order to provide oxygen and nutrients to every cell. Heart function disorders leads to serious problems. According to World Health Organization, globally more people die from cardiovascular disease than for any other cause. In 2004 more than 17.7 million people died from heart dysfunction, accounting for 30% of deaths. It is estimated that in 2030 it will be 23.6 million people.

A good comprehension of the function of the heart can improve the health and prevent disease. Especially, efforts should be put to describe the influence of diverse drugs(1–5) and compounds which form human diet(6–10). Health care should be personalized to each patient with respect to his state, genetic predisposition and other factors. This way it would be possible to improve the quality of life of patients and decrease the number of deaths from cardiovascular diseases. The cardiac modelling is one of the tools used to study the heart function.

The mechanism of heart contraction is very complex. The control of its activity is not conscious but is driven by the conduction system of the heart, and the contraction is tightly coupled with electrophysiology. The underlying mechanisms of the electro-mechanical coupling are not yet fully understood.

The electrical activity of the heart can be studied at several levels. The base level is the molecular one. In the cell bilipid membrane are incorporated a variety of types of proteins. Some of them are permeable to ions. These are denoted as ion channels. Every type of ion channel is selective to a specific type of ions. The permeability of the majority of channels depends on the membrane potential. There are several types of channels. The most important are the sodium (Na^+), potassium (K^+) and calcium (Ca^{+2}) channels.

The channels are voltage-gated, meaning that depending on the membrane potential the probability of channels to be in the open or close state changes. In the open state ions can pass through the channel driven by the electrical gradient, concentration gradient or both. When the cell is electrically stimulated the membrane potential changes. If this change reaches a threshold the cell is rapidly depolarized and then repolarized. This phenomenon is called action potential (AP).

In the cardiac tissue the cells are connected by gap junctions. Through gap junctions the stimulus can pass from one cell to the near-by cells. In this way the whole heart can be depolarized. In the heart there are also isles of tissue which are depolarizing spontaneously. The most important one is the sinoatrial node which has the pacing function in the heart.

At the macroscopic level the electrical activity of heart can be registered on the surface of the body. The name of this technique is Electrocardiography (ECG). The ECG were registered and described in the beginning of the 20^{th} century by the Nobel Prize laureate Willem Einthoven.

The approach in this work is to describe mathematically the physiological and anatomical reality of the cardiac cell. With the advantages of computational technology it is easier than ever before to simulate the behaviour of the cardiac channel, cell, tissue or

even of the whole heart. This computational approach can help to understand how the heart works. Recently models of cardiac cells of experimental animals cells were published as a mouse model by Kharche at al.(11), dog model by Hund at al(12) or rabbit model by Shannon at al.(13). Also various human cell models were developed(14–16).

The consumption of fish has beneficial effect to the heart function due to polyunsaturated fatty acids (PUFA)(6–8; 17; 18). The PUFA shorten human AP (8; 9; 19; 20) by influencing other cardiac channels. To simulate these effects is necessary understand the effect on each of the cardiac ion channel. This work is focused on simulation of the influence of the polyunsaturated fatty acids (PUFA) on the I_{Ks} channel.

Experimental data for this work were obtained from another lab (Instituto de Investigaciones Biomédicas "Alberto Sols" CSIC-UAM, Madrid, Spain)(21). The data were obtained from voltage-clamp experiments on cells transfected with a gene coding I_{Ks} channel (KCNQ1-KCNE1). Measurements were performed after Acute and Chronic 48 hours lasting exposure to eicosapentaenoic acid (EPA) and Acute exposure to docosahexaenoic acid (DHA).

The experimental data were used as a target in parameter identification of the 17 states Markov chain model proposed by Silva and Rudy(22). Nelder-Mead simplex algorithm(23) was used to estimate 15 parameters of the model. The ordinary differential equation (ODE) solver was used to get stable solution. The appropriate parameter set was identified for each case. Further, it also included the altered model of I_{Ks} into human ventricular models.

1.1 Effects of ω3 Polyunsaturated Fatty Acids on Cardiac Cells

The function of the heart is influenced by drugs but also by compounds in food. The American Heart Association recommends consuming two portions of fish every week, especially fish rich in ω-3 polyunsaturated fatty acids (PUFA). The hypothesis of the beneficial effects of fish oil was established after observing that the Eskimos which have diet rich on fish don't suffer of sudden cardiac death. Interestingly, further investigations have described contrary effects in patients with angina pectoris(8; 17).

Omega-3 polyunsaturated fatty acids (ω3-PUFA) constitute several unsaturated fatty acids. These acids are essential for normal growth and good health. The alimentary source of ω3-PUFA is mainly fish but in small range they are also in other types of meat, eggs, algae, nuts and other sources. The benefit of ω3-PUFA to health has been a subject of many studies. They described anti-cancer effects(18; 24; 25) , positive effect on neurology(26) and immune function, but the main benefit of PUFA is on the heart (6–10; 19; 20; 27–29). EPA and DHA are considered as the ω3-PUFA with the most benefit to the heart.

The action of PUFA in cardiac cell depends on the duration of exposure. The effects of PUFA are summarised in Table 1.

ω3-PUFA	Acute	Chronic
Membrane currents		
I_{Na}	Reduction(30–32)	Unchanged(33; 34)
I_{CaL}	Reduction(35; 36)	Reduction(33)
I_{K}	Reduction(37)	Not reported(33)
I_{Kr}	Reduction(6)	Unchanged(33)
I_{Ks}	Increase(38)	Increase(33)
I_{K1}	Unchanged(37)	Increase(34)
I_{to1}	Reduction(39–41)	Unchanged(33)
I_{NXC}	Reduction(42)	Reduction
Calcium homeostatic		
Resting $[Ca^{2+}]_i$	Reduction(43; 44)	Unchanged(33; 45)
$[Ca^{2+}]$ transient	Reduction(36; 43)	Unchanged(33)
Sarcoplasmic reticulum Ca^{2+} content	Increase(44; 46; 47)	Unchanged(45)
Spontaneous Ca^{2+} release	Reduction(43; 44; 46)	Not reported
Ca^{2+} sparks	Reduction(36; 44)	Not reported
Ryanodine receptors	Reduction(46; 48)	Not reported

Table 1: Summary of effects of PUFA to current densities and Ca^{+2} handling (8).

1.1.1 Experimental Data – PUFA Modulation of I_{Ks}

The experimental data set was kindly provided by Carmen Valenzuela, Ph.D. (Instituto de Investigaciones Biomédicas “Alberto Sols” CSIC-UAM, Madrid, Spain)(21).

The experiments were performed on African green monkey kidney-derivated cell line. The cells were transfected with human gen coding I_{Ks} (KCNQ1 - KCNE1). The experiments were performed in control condition, and in presence of EPA and DHA PUFAs both in concentration of 20 μmol/l. The available measurements were performed after Acute and Chronic (48 hours lasting) exposure.

The membrane currents measurements were performed using patch-clamp technique with aphotericin B-perforated patch configuration(3; 49). The Axopatch 200B amplifier was used to record the currents. Currents were filtered at 1 kHz by 4-pole Bessel filter and sampled at 2 kHz. Capacitance and serial resistance were digitally compensated. The measurements were performed at room temperature (21-23ºC).

Three current-voltage (I-V) protocols were used. In all protocols the cells were held at holding potential of -80 mV for a duration of 25 s. This allowed complete deactivation of the I_{Ks} channel. Then the currents were measured under various values of depolarizing voltage (testing potential) for a duration of 5.5 s or 12.5 s. The potential of

-40 mV was applied after the depolarizing pulse to perform the repolarization current measurement.

The experimental data are presented as the mean current traces. Figure 1 shows the I-V multiple-traces for all four cases.

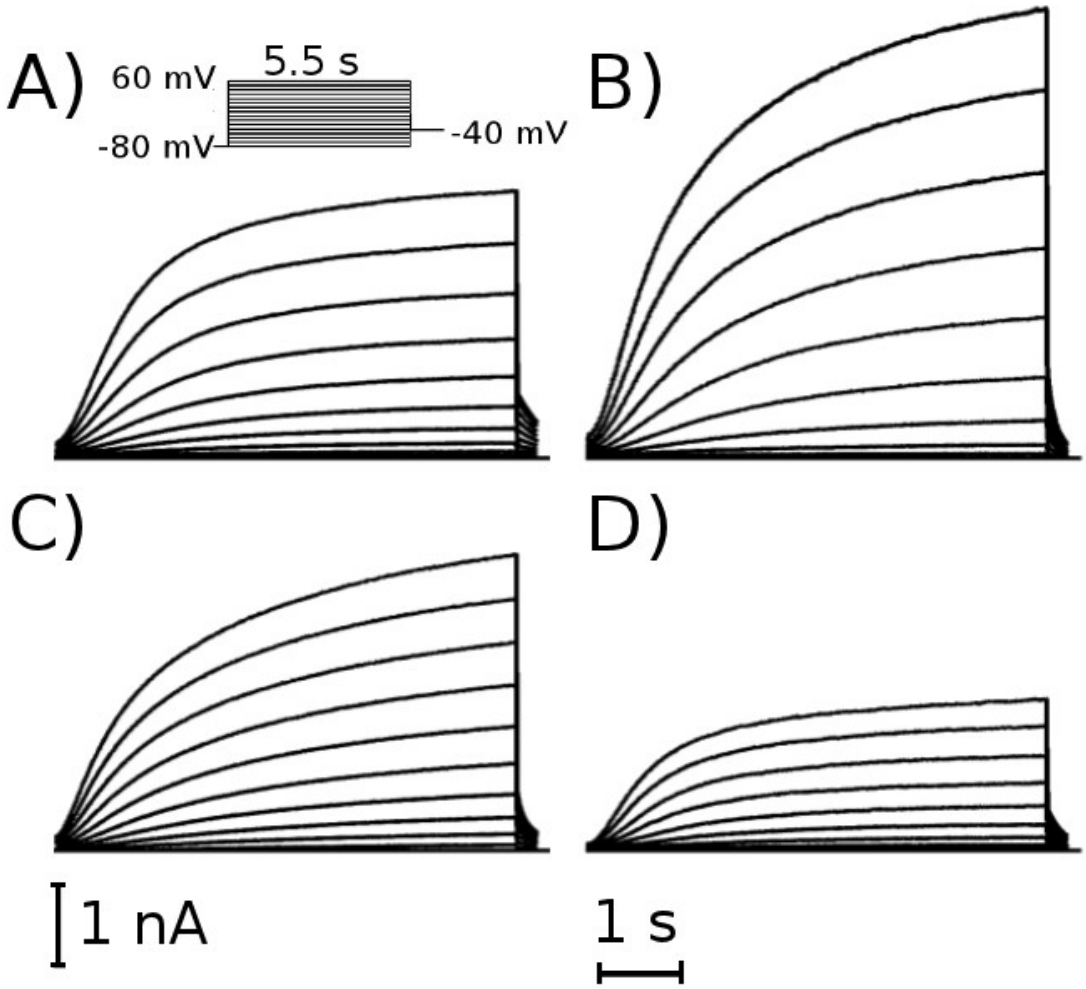

Figure 1: Mean experimental traces in response to the I-V protocol.

The 5.5 s pulses from holding potential of-80 mV to test potential in range of -80mV to 60mV followed by repolarization to -40mV were applied in steps of 10 mV (panel A, inset). A) Control current traces (n=9) B) Acute DHA (n=4) C) Acute EPA (n=5) and D) Chronic EPA (n=4).

The test potential was applied for the duration of 5.5 s. The value of the test potential ranged from -80 mV to the highest value of 60 mV in steps of 10 mV. The tail current was recorded for a duration of 0.25 s. The measurement was performed in Control condition and after Acute DHA, Acute EPA and Chronic 48 hours lasting EPA exposure. The higher testing potential value corresponds to the higher current value. The depolarizing current increased monotonically in all cases. There was no inactivation during test pulse. The depolarization was slow. The repolarization decreased monotonically.

The short single traces are shown in figure 2. The data are presented as the mean current traces. The cells were held at the potential of -80 mV. Than the 60 mV test potential was applied for a duration of 5.5 s. The tail current was recorded for a duration of 2 s at the potential of -40 mV. The short single trace measurements were performed in Control condition, after Acute DHA, Acute EPA and after Chronic 48 hours lasting EPA exposure.

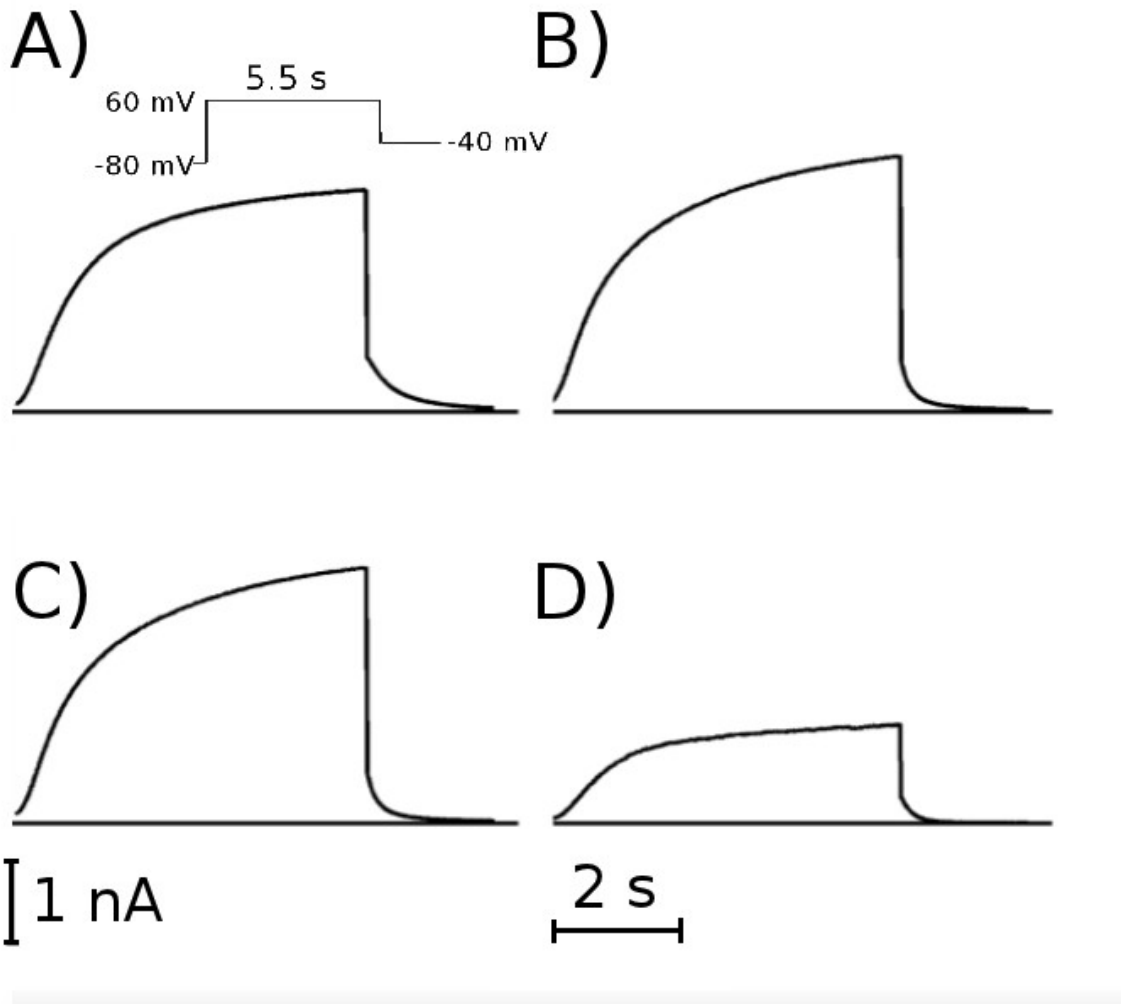

Figure 2: Mean experimental traces in response to short depolarizing protocol.

Single 5.5 s pulse is applied from holding potential of -80 mV to 60 mV followed by repolarization to -40 mV (panel A, inset). A) Control (n=23) B) Acute DHA (n=11) C) Acute EPA (n=12) and D) Chronic EPA (n=4).

The long depolarizing single traces current is shown in figure 3. The data are presented as the mean current traces. As in previous protocols cells were held on the potential of -80 mV. Then the 60 mV test potential was applied for a duration of 12.5 s. The relatively long duration of the depolarization helps to reveal slow kinetics of the I_{Ks} channel. The tail current was recorded for a duration of 2 s at the potential of -40 mV. Long single trace measurements were performed in Control condition and after Acute DHA and Acute EPA exposure. There are no data for Chronic EPA exposure.

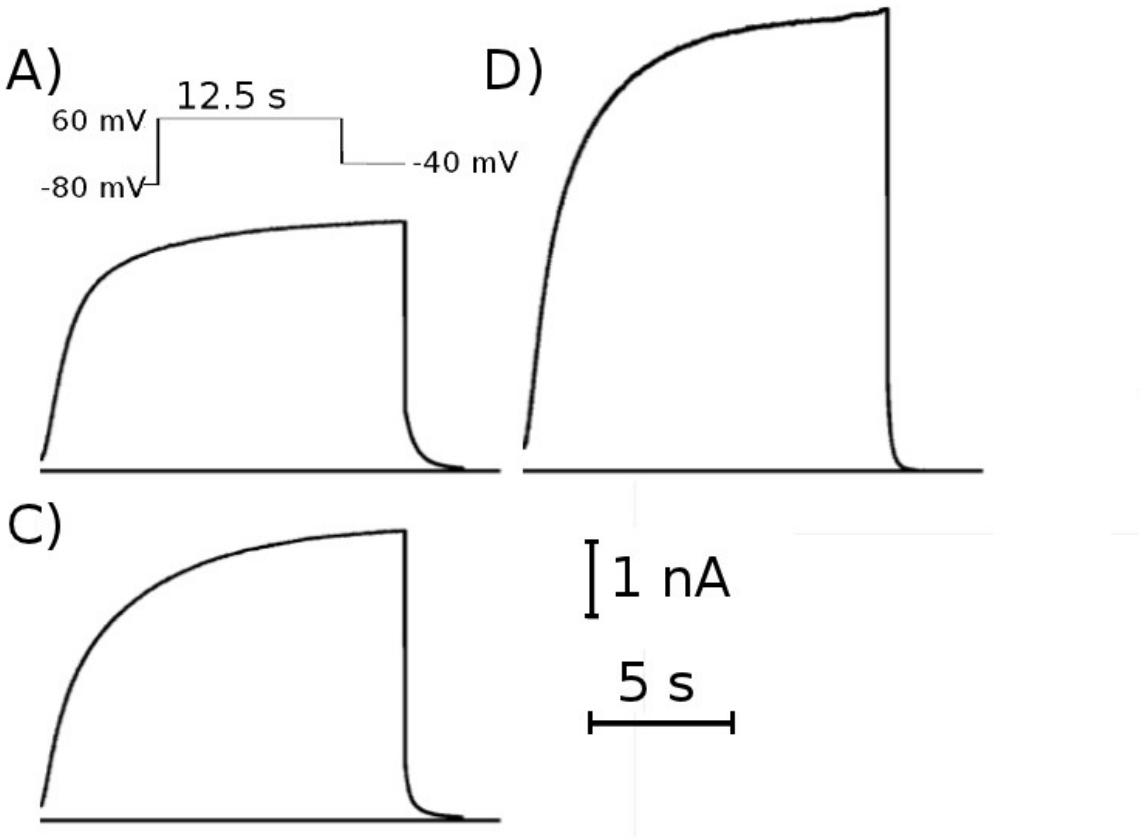

Figure 3: Mean experimental traces in response to long depolarizing protocol.

Single 12.5 s pulse is applied from holding potential of -80 mV to 60 mV followed by repolarization to -40 mV (panel A, inset). A) Control (n=9) B) Acute DHA (n=4) C) Acute EPA (n=5). There is no 12.5 s trace for the Chronic EPA.

1.2 Cardiac Modelling

The understanding of heart function and of the mechanisms underlying its disorders is fundamental for effective treatment. In this framework the cardiac modelling studies help to describe the heart function.

The computational models of human heart are well established tool for the research for a number of reasons. First, obtaining human myocytes for electrophysiology experiments is complicated. Second, the animal myocytes used for experiments may have different features. Finally, computational modelling provides information which in experimental observation would be inaccessible or their acquisition would be very technically challenging.

To reproduce the AP propagation in the heart we need the integration of diverse models. The anatomical model provide information about the shape of the heart and tissue model define location of different types of cardiac cells. In particular, there are three basic types of cells in myocardial wall, which may differ significantly in specific current densities. Epicardial cells form the outside part of the heart wall. Endocardial cells are

located inside the heart. The interstitial space is filled by M cells. Auto-stimulated cells are responsible for the pace making of the heart. The most important of them are located in the sinoatrial node.

Fibre orientation is another very important feature which is incorporated in the geometry model. The propagation is not spatially homogeneous but it differs depending on the diffusion. This aspect is conditioned by the orientation of the tissue fibres and gap-junctions between cells. The geometry and tissue models are based on advanced image acquisition techniques like computed tomography (CT), magnetic resonance (MRI) and diffusion tensor MRI (DT-MRI).

The simulations of whole heart are very time-demanding. The simulation of few seconds of heart activity would require years of simulation on current PC. The code is usually divided between various processing units and the computation is done in parallel(50). The complexity of 3D whole heart model requires more assumption which leads to uncertainties on the result. The cell model may facilitate the model validation. One dimensional and two dimensional models could give us basic idea about the heart tissue behaviour with the advantage of lower cost on the computational capacity.

1.2.1 Models of Human Ventricular Cell: Basal Models and Pacing Behaviour

The computational models implement a mathematical description of the cell and its subunits. The model is usually based on a system of ODEs. The models also count with the spatial dimensions, cellular organelles, and other aspects of the cellular environment. The goal of the cell model is to simulate the electrical behaviour of the cell. The validation of cell model could be done against single cell experiments which are easy to obtain. Together with the models of tissue the cell and heart geometry, they provide tool to study the mechanisms of the life-threatening arrhythmias.

1.2.2 Models of Ion Channels

The cell membrane is a bilipid layer separating the intracellular and extracellular space. The intracellular and extracellular spaces have different ion concentrations. Alteration of ionic concentrations out of the physiological limits may lead to modifications of AP that can result in arrhythmias(51–53). Changes in ion concentration are usual in patients with alteration of renal function who have to undergo hemodialysis(54).

Na^+ and Ca^{+2} concentrations are higher outside of the cell while the K^+ concentration is higher inside of the cell. These concentration differences are maintained by the sodium-potassium pump which uses the energy from adenosine triphosphate (ATP). In the steady-state condition the potential of the membrane is about -80 mV. This is denominated resting potential. In the cellular membrane are incorporated large proteins molecules which can be selectively permeable to some types of ions. Such proteins are called ion channels.

Figure 4 shows the schema of the cell membrane from the electric point of view. The permeability of ion channels depends on the membrane potential and others factors. When the cell potential increase (becoming less negative) the Na^+ channel becomes open

(activated). By the concentration and potential gradient the Na^+ ions flow rapidly into the cell. This Na^+ influx makes a membrane potential more positive which inactivate the Na^+ channel. The increasing membrane potential activates the potassium channel and the outflow of K^+ tends to repolarize the cellular membrane back to the resting potential. This mechanism of depolarization and repolarization is denoted as action potential (AP).

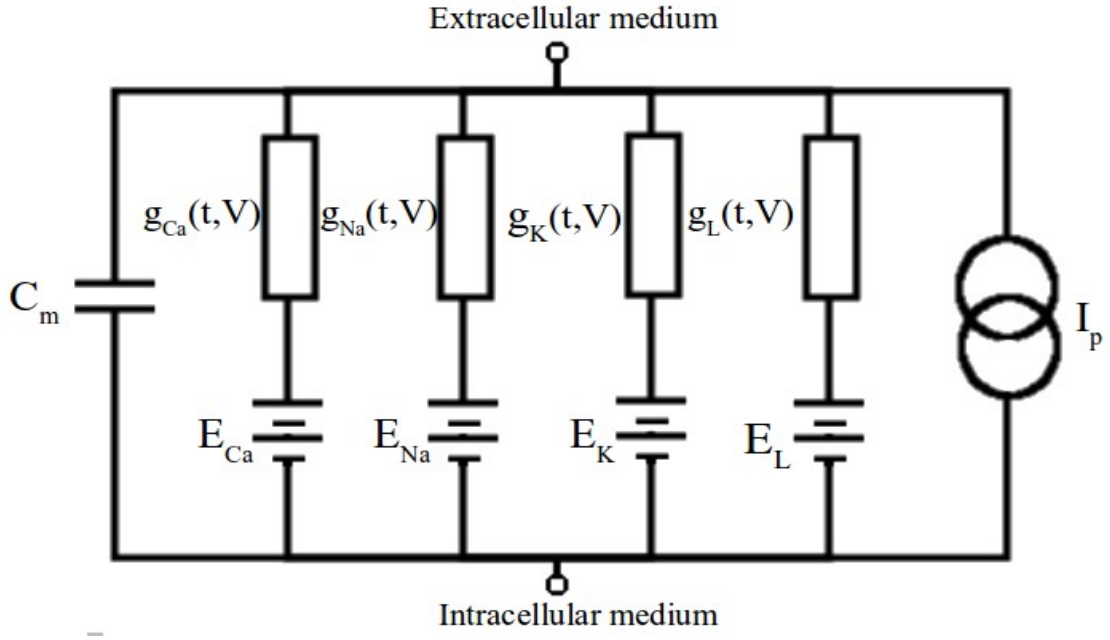

Figure 4: Electrical scheme of cell model.

The scheme represents the electrophysiological model of the cell membrane. The C_m is the capacitance of the membrane. The conductance of the ionic channel is represented by g(t,V). The conductance depends on time t and membrane potential V. The electrochemical gradient driving is represented by E. In the model are represented three main ionic currents- Ca^{+2} current I_{Ca}, Na^+ current I_{Na}, K^+ current I_K. The I_L represents leakage current which is a summary of effects of other minor currents. The current source I_p is a representation of pumps and exchangers.(55)

The gating mechanisms of the ion channels were discovered by Hodgkin and Huxley in 1952(55). They studied various types of channels of squid giant axon. They described the underlying mechanism of AP by the differential equations. They induced model of ion channel based on voltage-gated activation and inactivation gates. The open probability of the activation gate increases with increasing membrane potential. The open probability of inactivation gate decreases with increasing membrane potential. The specific channel properties can be reached by combinations of a number independent activation and inactivation gates. This model is widely used in cardiac cell models but it has several limitation in reproducing some features of ion channels. This can be resolved by another type of model which is denoted Markov chain model.

Markov chain is a mathematical system that can change its state from one state to other in a chain-like manner(56). The probability of the transition does not depend on the previous state of the system. It is named after the Russian mathematician Andrey Markov (1856 - 1922). This system is widely used in a number of application as a statistical model. The states may be linked to the molecular dynamics of the channel(57).

Ca^{+2} plays an important role in muscular cells because it drives the contraction of the cell. The Ca^{+2} specific channel is present in the muscular cells. The Ca^{+2} concentration is higher in extracellular space. The sarcoplasmic reticulum provides an intracellular Ca^{+2} reserve. During AP the Ca^{+2} flow inside the muscular cell. Increasing intracellular concentration of Ca^{+2} induces the release of the sarcoplasmic Ca^{+2}. When the Ca^{+2} concentration increases, the cell is contracted.

1.2.3 Arrhythmogenic Mechanisms

Sudden cardiac death arises from arrhythmias. The two main arrhythmogenic mechanisms are triggered activity and reentry. The probability of suffer arrhythmias increase during myocardial ischemia(58; 59). The benefit of PUFA depends on underlying mechanism of the pathology.

The triggered activity is abnormalities in the impulse initiation (Figure 5, panel a,b). They usually arise from early and delayed after depolarizations (EAD and DAD). EAD occurs in slow cardiac rhythm when AP is prolonged. In this case the depolarizing currents that were inactivated in the beginning of AP are activated again making arise the potential. The EAD can lead to a particular tachycardia named Torsade des Pointes because of its characteristic appearance on ECG. The clinical treatment is AP shortening.

The DAD occurs in the rapid cardiac rhythm when intracellular Ca^{+2} is elevated. That leads to overcharging of intracellular organelle named sarcoplasmic reticulum. The sarcoplasmic reticulum drives the muscular contraction. When the overcharging occurs it can not sustain Ca^{+} and releases it in an incorrect instant. That increases the potential. If the threshold is reached it may initiate AP propagation end reentry. The DAD are treated by AP shortening, slowing heart rate, reducing Ca^{+} concentration and decreasing cardiac excitability.

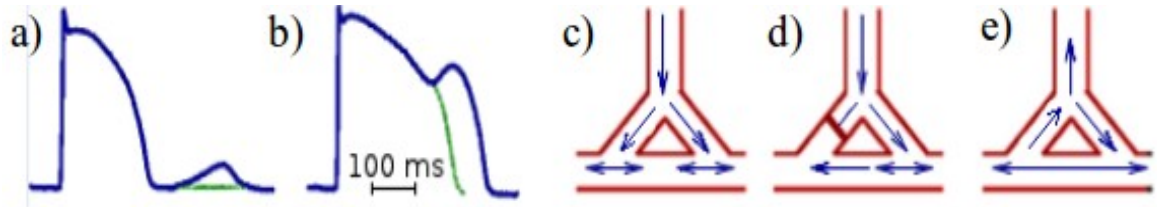

Figure 5: Arrhythmia mechanisms.

a) and b) show triggered activity. Blue lines denoted the pathological AP. Green lines denotes the difference between pathological and physiological AP. a) DAD may arise during rapid cardiac rhythms when the Ca^{+} concentration is elevated. b) EAD may arise when AP is prolonged during slow cardiac rhythm. c), d) and e) show reentry mechanism. The normal conduction c) starts in sinus node end ends after repolarizing whole heart. After unidirectional block which is shown on panel d) the impulse may lead to re-entrant auto-maintained circuits shown on panel e).

The second group of arrhythmias are the reentrant arrhythmias due to unidirectional block (Figure 5, c, d, e). In normal heart the impulse is generated in the sinus node. The impulse ends after depolarizing whole heart. After an unidirectional block of the impulse the same impulse may continue to re-excite the heart tissue. That may occur when the conduction velocity is slow and refractory period is short.

The interventions aimed to treat arrhythmia differ depending on its mechanism. Actions leading to treat one type of arrhythmia may be pro-arrhythmic in arrhythmias caused by other mechanism. For this reason is very important to know the underlying mechanism in each case.

1.3 The KCNE1-KCNQ1 Channel, I_{Ks} Current, and Its Models

The I_{Ks} is the slowly activated delayed rectifier potassium channel which plays important role in the cardiac cell repolarization. The malfunction of I_{Ks} channel leads to arrhythmias(60). I_{Ks} is even more important in the case of drug stimulaton(4) or gene mutations(61; 62). Moreover, the I_{Ks} can sustain repolarization in case of dysfunction of other K^+ channels.

The concentration of K^+ in the intracellular space of the living cells is higher than in the extracellular space. This difference tends to be equilibrated by the releasing of K^+ into extracellular space. The release is driven by the concentration gradient. Another force which causes release of K^+ is based on the potential gradient. The resting potential of the cell is normally about -80 mV. Since the ions of K^+ carry positive charge they tend to move outside. There are various type of channels selective to K^+ (I_K, I_{K1}, I_{Kr}, I_{Ks}).

Figure 6 shows a Hodgkin-Huxley type model of I_{Ks}. There are two independent activation gates and no inactivation gate in this model(63; 64). There were used also models with three identical activation gates in some studies(65). The model in Figure 6 is described by the Equation 1 (64).

$$I_{Ks} = G_{Ks} \cdot \left(1 + \frac{0.6}{1 + \left(\frac{3.8 \cdot 10^{-5}}{[Ca^2]} \right)^{1.4}} \right) \cdot x_{s1} \cdot x_{s2} \cdot (V_m - E_K) \qquad \text{Equation 1}$$

Where G_{Ks} represent the conductance of I_{Ks} channels when are all open. The V_m represent the membrane potential and E_K is the Nerst potential of K^+ which depend on the intra and extracellular concentration of the K^+. The difference between $V_m - E_K$ is denominated driving force. The x_{s1} and x_{s2} variables describing the gating mechanism of the channel gates. The x_{s1} and x_{s2} represent the probability, that specific channel gate is open.

The maximal conductance G_{Ks} is mainly connected with the total number of channels. When the cells are dissociated during the preparation for path-clamp experiments many I_{Ks} channels are destroyed. The real number of channels in the cell model has to be estimated. The estimation give rise to uncertainties and so value of G_{Ks} vary hugely depending on the model.

It is supposed an existence of two independent non-identical gates in the current O'Hara et al. model(14). The gate x_{s1} control the activation. The gating properties are described by the Equation 2. The gating of x_{s2} gate controlling deactivation is defined analogically.

$$\frac{dx_{s1}}{dt} = \frac{x_{s1,\infty}(V_m) - x_{s1}(t)}{\tau_{x,s1}(V_m)} \quad \text{Equation 2}$$

Where $x_{s1,\infty}(V_m)$ represent steady-state probability of opening at specific membrane potential and the $\tau_{x,s2}(V_m)$ is time constant of the system.

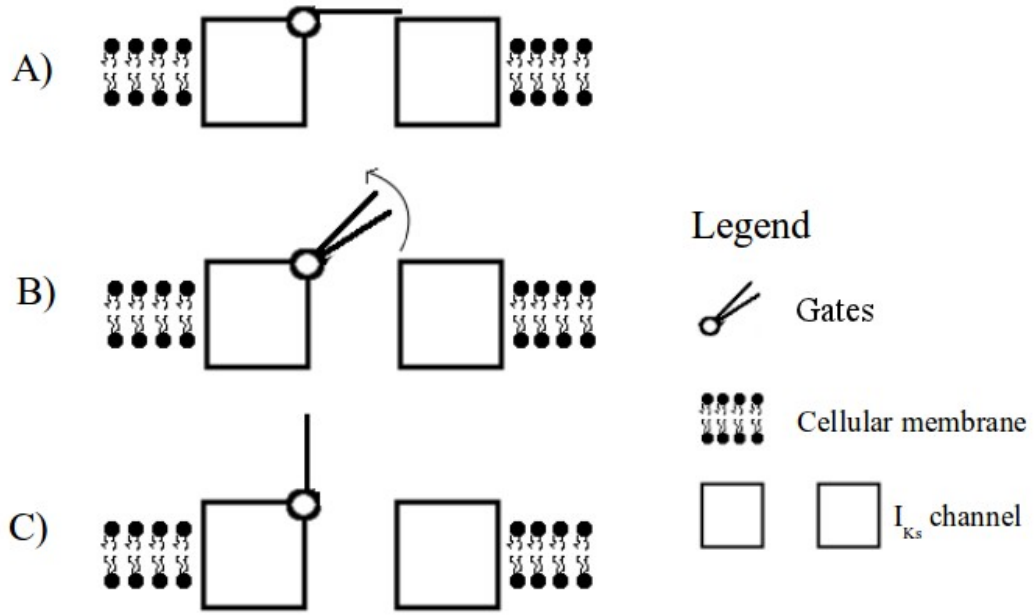

Figure 6: I_{Ks} model - Hodgkin - Huxley type.

In this figure is shown the model of I_{Ks} channel according to the model developed by Hodgkin and Huxley. The model contains two gates. The channel is close if at least one of the gates is close. The channel is open only when both gates are open. Picture A) shows closed channel. Picture B) shows channel being opening. Picture C) shows opened channel.

Silva and Rudy in Circulation 2005 proposed more detailed description of the I_{Ks}(22) using Markov chain model. In further study they linked the molecular dynamic and electrostatics to the states of the Markov chain model(57). According to the chemical structure there are 4 subunits in the I_{Ks} channel. When the channel is closed each subunit can be in one of three conformations denoted by R_1 (deep closed), R_2 (intermediate closed), A (activated state). If all the subunits are in the activated state the channel can be opened (states O_1 and O_2).

Figure 7 shows the abbreviated form of the Markov chain. Each of the subunits can be in one of three conformational states and can undergo to others states with a voltage-dependent transition rates. The subunit in R_1 state it can do a transition to R_2 with the transition rate α. The subunit in R_2 state can undergo transition to R_1 with the transition rate β or the transition to activated state A with the transition rate γ. The transition from the state A to R_2 is characterized by the transition rate δ.

If all the subunits are in the activated state A, they can undergo a transition to an open state O_1 with a transition rate θ. Unlike other voltage -dependent transition, this

transition is voltage-independent. The reverse transition has a transition rate η and is voltage dependent. The transition to the other open state O_2 is characterized by the transition rate ψ and reverse transition by transition rate ω. The transition between states depend exponentially on the membrane potential.

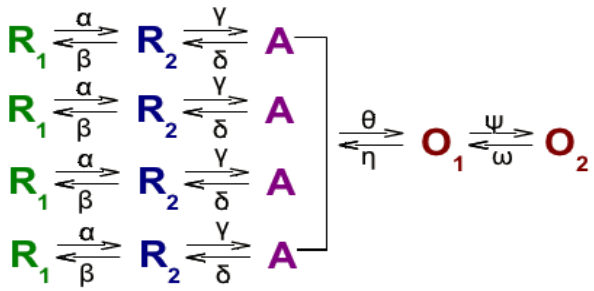

Figure 7 Markov chain model of the I_{Ks} channel (abbreviated form).

The abbreviated form of the Markov chain model of I_{Ks} channel shows the conformational changes of each of the four subunits (in lines).

Table 2 shows the equations describing the transition rates. The multipliers m_i are positive unit-less number. The exponent parameters p_i are in ms^{-1}. The p_i of the transition leading to open-state is positive while the p_i of the transition leading to closed state is negative.

$\alpha = m_1 e^{\frac{p_1 V F}{RT}}$	$\beta = m_2 e^{\frac{p_2 V F}{RT}}$	$\theta = m_5$	$\eta = m_6 e^{\frac{p_5 V F}{RT}}$
$\gamma = m_3 e^{\frac{p_3 V F}{RT}}$	$\delta = m_4 e^{\frac{p_1 V F}{RT}}$	$\psi = m_7 e^{\frac{p_6 V F}{RT}}$	$\omega = m_8 e^{\frac{p_7 V F}{RT}}$

Table 2: Markov chain transition rates.

The parameters m_1-m_8 are the multipliers (arbitrary units). The multipliers are always positive. The parameters p_1-p_7 are the exponents (ms^{-1}). The first two columns show the transition rates which leads to open states. The second two columns show the transition rates which leads to states R_1 of the subunit.

The complete Markov chain structure is shown in Figure 8. It contains 15 closed states to account all the combinations of of states on each of four subunits. The first closed state C_1 is the state where all 4 subunits are in the R_1 state. In C_2 one of the subunits is in the R_2 state while other 3 subunits in R_1 state. The probability of transition from C_1 to C_2 is 4α since there are 4 subunits that can do this transition.

The channel in state C_2 can do the reverse transition to C_1 with the probability β (only one subunit was in R_2 state). The transition to C_3 with the probability 3α (subunits were in R_1 state) or transition to C_6 with probability γ (one subunit was in R_2 state). The transitions from other states are analogous to the described transition from C_1 and C_2.

The transition in row means the first transition (from R_1 to R_2) of some of the subunit. The transition in column means the second transition (from R_2 to A) of some of

the subunit. When all subunits are in state A (state C_{15} in complete model form) they can do cooperative voltage-independent transition to open states.

The states occupancies are described by the ODEs which are shown in Table 3.

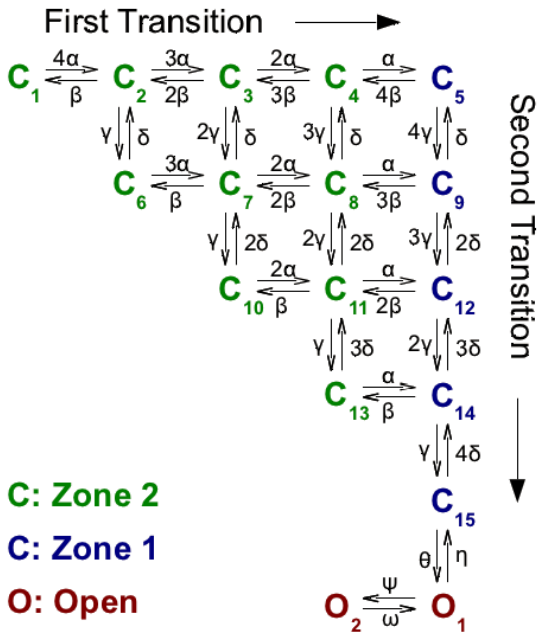

Figure 8: Markov chain model of I_{Ks} (complete form).

I_{Ks} Markov model contains 15 closed states (from C_1 to C_{15}) and two open states (O_1 and O_2). Green Zone 2 represents close states where at least one of the four subunits remains in R_1 state. Blue Zone 1 represents close states that have complete the first transition for all subunits. There are two open states (red).

$$\frac{dC_1}{dt} = \beta \cdot C_2 - 4\alpha \cdot C_1$$

$$\frac{dC_2}{dt} = 4\alpha \cdot C_1 + 2\beta \cdot C_3 + \delta \cdot C_6 - (\beta + 3\alpha + \gamma) \cdot C_2$$

$$\frac{dC_3}{dt} = 3\alpha \cdot C_2 + 3\beta \cdot C4 + \delta \cdot C_7 - (3\beta + 2\alpha + 2\gamma) \cdot C_3$$

$$\frac{dC_4}{dt} = 2\alpha \cdot C_3 + 4\beta \cdot C_5 + \delta \cdot C_8 - (3\beta + \alpha + 3\gamma) \cdot C_4$$

$$\frac{dC_5}{dt} = \alpha \cdot C_4 + \delta \cdot C_9 - (4\beta + 4\gamma) \cdot C_5$$

$$\frac{dC_6}{dt} = \beta \cdot C_7 + \gamma \cdot C_2 - (3\alpha + \delta) \cdot C_6$$

$$\frac{dC_7}{dt} = 3\alpha \cdot C_6 + 2\beta \cdot C_8 + 2\gamma \cdot C3 + 2\gamma \cdot C_{10} - (\beta + 2\alpha + \delta + \gamma) \cdot C_7$$

$$\frac{dC_8}{dt} = 2\alpha \cdot C_7 + 2\beta \cdot C_9 + 3\gamma \cdot C_4 + 2\delta \cdot C_{11} - (2\beta + \alpha + 2\gamma + \delta) \cdot C_8$$

$$\frac{dC_9}{dt} = \alpha \cdot C_8 + 2\delta \cdot C_{12} + 4\gamma \cdot C_5 - (3\beta + \delta + 3\gamma) \cdot C_9$$

$$\frac{dC_{10}}{dt} = \beta \cdot C_{11} + \gamma \cdot C_7 - (2\alpha + 2\delta) \cdot C_{10}$$

$$\frac{dC_{11}}{dt} = 2\alpha \cdot C_{10} + 2\beta \cdot C_{12} + 2\gamma \cdot C_8 + 3\delta \cdot C_{13} - (\beta + \alpha + \gamma + 2\delta) \cdot C_{11}$$

$$\frac{dC_{12}}{dt} = \alpha \cdot C_{11} + 3\delta \cdot C_{14} + 3\gamma \cdot C_9 - (2\beta + 2\delta + 2\gamma) \cdot C_{12}$$

$$\frac{dC_{13}}{dt} = \beta \cdot C_{14} + \gamma \cdot C_{11} - (\alpha + 3\delta) \cdot C_{13}$$

$$\frac{dC_{14}}{dt} = \alpha \cdot C_{13} + 4\delta \cdot C_{15} + 2\gamma \cdot C_{12} - (\beta + 3\delta + \gamma) \cdot C_{14}$$

$$dC_{15} = \gamma \cdot C_{14} + \eta \cdot O_1 - (4\delta + \theta) \cdot C_{15}$$

$$\frac{dO_1}{dt} = \theta \cdot C_{15} + \omega \cdot O_2 - (\psi + \eta) \cdot O_1$$

$$\frac{dO_2}{dt} = \psi \cdot O_1 - \omega \cdot O_2$$

Table 3: Rate of change equation for state occupancies.

The equations describe the dynamics of state occupancies and their dependence on transition rates. The $C_{1\text{-}15}$ denote closed states. The $O_{1\text{-}2}$ denote open states.

1.4 Algorithm for Identification of Model Parameters

Mathematical models are used in many branches of science and industrial application. Models based upon stiff ODEs are usual in biology and life sciences. The ODE solvers are part of variety of mathematical tools and programme libraries.

Such systems are described by variety of independent parameters. All the parameters have influence to the behaviour of the model. The identification of model parameters is very common but technically challenging and computationally demanding task. There is variety of minimum searching methods. Widely used algorithm for nonlinear minimum searching is the Nelder-Mead simplex method(23). This method was successfully used in previous studies of I_{Ks}(4; 22; 61). The method was published in 1965 by J. A. Nelder and R. Mead. Since then the simplex algorithm was widely used in both industry and science. Further the method was improved(66; 67) to reach even better parameter identification.

The algorithm for identification of model parameters could be developed in any appropriate programming language. Prepared libraries contain variety of mathematical operations and other function such as ODE solvers and minimum searching methods which can be included to the algorithm.

1.4.1 The Nelder-Mead Simplex Method

The simplex method for function minimization is an algorithm used to find the minimum a function of n variables. The method uses a simplex to reach compact and computationally effective algorithm. Simplex is a generalization of the notion of triangle or tetrahedron to arbitrary dimensions. The simplex is defined by (n+1) vertices which are the points from n dimensional parameter space. The function to minimize is denoted cost function.

The algorithm flow is shown in Figure 9. The simplex vertices (P_1, P_2, ..., P_{n+1}) and the cost function value in this points $f(P_i)$ are calculated at the initialization. Then the parameters are ordered according to the cost function values at the vertices. The P_1 denote the point with the lower cost function value (best point). The P_{n+1} denote the point with the highest cost function value (worst point).

The centroid $\overline{P}$ is denoted as the centre of gravity of all the points except the worst P_{n+1}. At each iteration the worst point P_{n+1} is replaced by a new point. The new point lies on the line joining the worst point P_{n+1} with the centroid $\overline{P}$. There are three operations used to obtain the new point – reflection, contraction and expansion.

The first operation is the reflection P_{n+1} denoted as P_R and its coordinates are defined by the Equation 3. If the cost function value of the reflected point $f(P_R)$ is better than the second worst $f(P_n)$ but not better than the best $f(P_1)$, than the worst point P_{n+1} is substituted by the reflected point P_R, and the algorithm starts again with the new simplex.

$$P_R = (1+\alpha)\cdot\overline{P} - \alpha\cdot P_{n+1} \quad \text{Equation 3}$$

P_R denotes the reflected point, $\overline{P}$ is defined as the centroid of all points except the worst P_{n+1}, α is a positive constant defined as reflection coefficient. The P_R lies on the opposite site than the P_{n+1} with respect to the centroid point $\overline{P}$.

If the cost function value of the reflected point $f(P_R)$ is lower than the $f(P_1)$ the algorithm continue searching another point. This operation is denoted expansion P_E and is defined by the Equation 4. If the function value of the expanded point $f(P_E)$ is less than the $f(P_R)$ than the worst point P_{n+1} is substituted by the P_E. In the contrary case the P_{n+1} is substituted by the reflected point P_R. And the algorithm starts again with the new simplex.

$$P_E = \gamma \cdot P_R + (1-\gamma) \cdot \bar{P} \quad \text{Equation 4}$$

P_E denotes the expanded point, P_R denotes the reflected point, $\bar{P}$ is defined as the centroid of all points except the worst P_{n+1}, γ is a constant greater than unity denoted as expansion coefficient. The P_E lies behind the P_R and on opposite site than the P_{n+1} with respect to the centroid point $\bar{P}$.

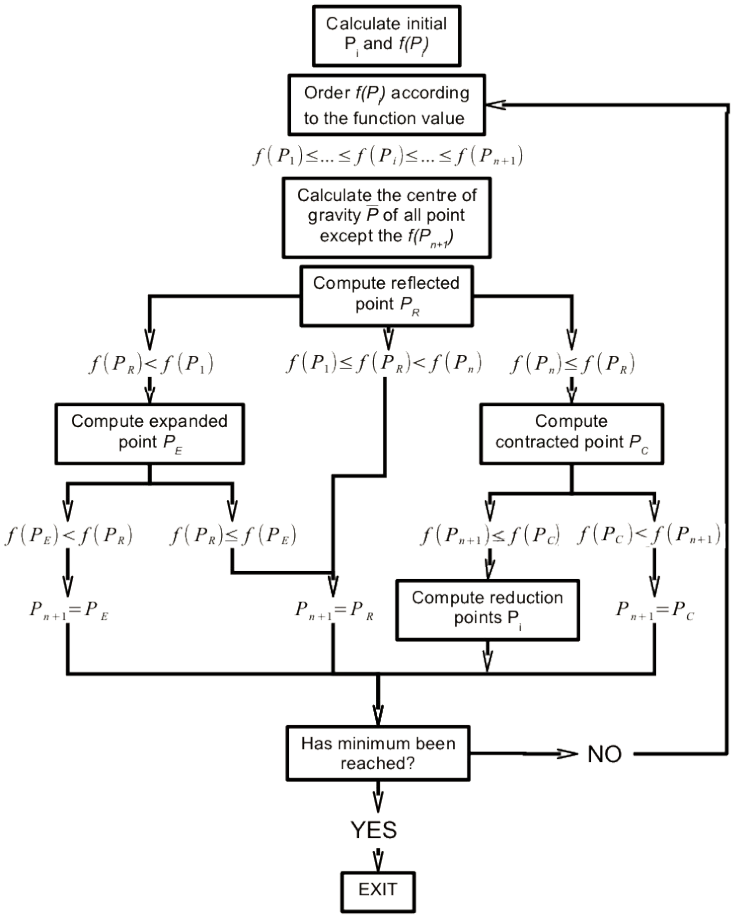

Figure 9: Flow diagram of the Nelder-Mead simplex method.

If the cost function value of the reflected point $f(P_R)$ is greater than the second worst point cost function value $f(P_n)$ than the algorithm continue searching another point. This operation is denoted contraction R_C and is defined by the Equation 5. If the cost function value of the contracted point $f(P_C)$ is lower than the worst point P_{n+1}, then this point is substituted by the P_C, and the algorithm starts again with new simplex.

$$P_C = \beta \cdot P_{n+1} + (1-\beta) \cdot \bar{P} \quad \text{Equation 5}$$

P_C is denoted the contracted point, $\bar{P}$ is defined as the centroid of all points except the worst P_{n+1}, β is a positive constant less than 1 defined as contraction coefficient. The P_C

lies between P_{n+1} and the centroid point $\overline{P}$.

If any of this operations does not lead to a better point than the worst point P_{n+1} than all P_i but the best point are replaced using an operation which is denoted reduction defined by the Equation 7, and the algorithm starts again with new simplex.

$$P_{Si} = P_1 + \sigma \cdot (P_i - P_1) \; for \; i \in \{2, \ldots, n+1\} \quad \text{Equation 6}$$

P_{Si} is the reduced parameter P_i, P_1 is the best parameter, σ is denoted shrink constant.

2 Methodology

2.1 Cell Culture

The cell line COS-7 derived from kidney of African green monkey was acquired from the American Type Culture Collection. The cell incubation was performed in nutrient mixture medium in 5% CO_2 atmosphere at physiological temperature (~37ºC). The nutrient mixture contained Dulbecco's modified Eagle's medium, 10% fetal bovine serum supplemented with antibiotics (100 IU/ml penicillin and 100 mg/ml streptomycin; all from Gibco, Paisley, UK).

The pCDNA3.1 KCNQ1-KCNE1 concatemer with reporter plasmid CD8 was introduced into the cell using lipid-based transfection reagent Fugene-6 (Roche Molecular Biochemical). Before experimental use cells were exposed to the anti-CD8 antibody as described previously(2; 68; 69).

2.2 Whole Cell Voltage Clamp

The whole cell measurements were performed to investigate the effects of PUFA to the I_{Ks}. The experiments were done at room temperature (~21-23ºC) under Control and in the presence of PUFA conditions. The modulation of I_{Ks} by various types of PUFA was studied. The experiments were performed under Acute and Chronic defined as 48 hours, of exposure to PUFA both at concentration 20 μmol/l. The PUFAs EPA and DHA (Sigma Chemicals, St.Louis, MO) were dissolved in ethanol (10 mmol/l) and properly protected from light and oxidation (nitrogen atmosphere at temperature of -20ºC) as described(6; 7).

Patch pipettes were fabricated from borosilicate glass capillary tubes (Narishige, GD-1, Tokyo, Japan), pulled on programmable horizontal puller (Sutter Instruments Co.,San Rafael, CA) and heat-polished with microforge (Narishige). The micropipette resistance ranged from 1 to 3 MΩ. The micropipette's internal filling solution was of the following composition (mmol/l): K-aspartate 80, KCl 50, phosphocreatine 3, $KH_2 PO_4$ 10, MgATP 3, HEPES-K 10, EGTA 5 (pH 7.25 adjusted with KOH). Cells were superfused with the bath solution contained (mmol/l): NaCl 130, KCl 4, CaCl2 1.8, MgCl2 1, HEPES -Na 10, and glucose 10 (pH 7.40 adjusted with NaOH) .

The measurements were done using the amphotericin B-perforated patch-clamp configuration(3; 49). The currents signals were acquired by an Axopatch 200B amplifier (Axon Instruments, Foster City, CA)(3) using pClamp version 9 software (Axon Instruments). Capacitance series resistance errors were reduced with electronic

compensation. Currents were filtered by four-pole Bessel low-pass filter and sampled at 2 kHz. The stimulation frequency was 0.03 Hz.

To obtain current voltage (I-V) the flowing voltage clamp protocol were used. The cells were held at holding potential of -80 mV for a duration of 25 s. This allowed complete deactivation of the I_{Ks}. After such a conditioning, activation pulse were applied from testing potential -80 mV to 60 mV in steps of 10 mV to elicit I_{Ks} current traces. These measurements quantified the kinetics of the activation evolution at various different potential values. The activation pulse was applied for 5.5 s to reveal the complete dynamics of I_{Ks} activation till up to it saturated at the given voltage. The deactivation of the I_{Ks} was then quantified by applying a repolarizing current pulse to -40 mV for a duration of 250 ms. The tail current so elicited quantified the deactivation. The activation duration of the multiple traces protocol was 5.5 s. The tail current duration is 250 ms. Current traces were registered for Control (n=9), Acute DHA (n=4), Acute EPA (n=5) and Chronic EPA (n=4).

Further, two single traces experiments were performed. These measurements quantified the very long term evolution of I_{Ks} at a high activating voltage. Similar to the I- V protocol the holding potential was kept at -80 mV. A single activating potential in these single trace experiments was taken to be 60 mV. The testing potential was applied for 5.5 or 12 s. The tail current was elicited upon return to potential of -40 mV. The shorter single trace activation duration was 5.5 s. The tail current duration was 1 s. Current traces were recorded for Control (n = 23), Acute DHA (n = 11), Acute EPA (n = 12) and Chronic EPA (n = 4). The longer single trace activation duration was 12.5 s. The tail current duration was 2 s. Current traces were registered for Control (n=9), Acute DHA (n=4), Acute EPA (n=5). There was no longer single trace for the Chronic EPA.

The raw numerical data were obtained in Microcal Origin 8.5 format (Microcal Software, Northampton,MA). Time, applied voltage and measured current in each step were registered with time step 0.25 ms. The data were exported by Origin to the text file.

2.3 Statistical Analysis and Preprocessing

The experimental data were analysed and processed using computational methods developed in house. The programming was carried out in Matlab (R2009a, The MathWorks, Natick, Massachusetts). The capacitive current spikes were removed from the traces. About 10 ms of capacitive current were removed in the beginning of the pulse and between the testing and return potential. The experimental data sets were processed separately for Control, Acute DHA, Acute EPA, and Chronic EPA cases. The mean values of the raw data were obtained for each time point of the traces.

The leak current was subtracted from the traces. The current value at first time point after the step from holding potential to the depolarizing potential (depolarizing step) was subtracted for whole depolarizing trace. The value at first time point after the depolarizing step to the testing potential of -40 mV was subtracted from all tail current records. The same procedure was applied for all cases with the specific leak current values. To our best knowledge there is no other study which subtracted leak current from COS cell line based I_{Ks} experiments. Thus, gating properties of leak current are not known, the leak current was subtracted as a constant at certain potential.

2.4 Parameter Identification

The Nelder-Mead algorithm for parameter identification was developed using pre-existing(4) and newly developed codes in Matlab. The I_{Ks} was simulated using the biophysically detailed 17 state Markov chain model by Silva and Rudy. The source code of the ion current model was obtained from the Rudy laboratory web pages(70).

A stiff ODE solver, which is implicit and recursive (defined by the function 'ode23s' in MATLAB), was used to integrate the I_{Ks} model. The algorithm uses a variable time step and gives stable solutions. Initial conditions of the ion current model were estimated by integrating the non-stimulated model at -80 mV for a prolonged duration (10000 s) and taking the final values of the state occupancies for initial conditions. Further, the system condition that the sum of all state occupancies is 1 was imposed.

The identification of the parameters of the model was done using Nealder-Mead algorithm(4; 23). The 15 independent parameters in the I_{Ks} model were identified for by the algorithm. All model parameters were allowed to be changed simultaneously during the algorithm iterations. The value of G_{Ks} which is mainly connected with the total number of channels was identified in Control case. The G_{Ks} was fixed to the control G_{Ks} in Acute cases. This was based on the assumption that in acute exposure the number of channels does not change. The 48 hours lasting exposure to EPA cause alteration of expression of I_{Ks} channels. The G_{Ks} was estimated from the experimental traces in Chronic EPA cases.

The simplex method is strongly dependent on the initial set of function parameters which is used to initialisation of the simplex vertices. The parameter set published by Silva and Rudy(22) was used as the initial guess in the identification runs. Since the cells were transfected with the gene which encodes human KCNQ1-KCNE1 the used parameter set was for human I_{Ks}.

All data points of the mean experimental traces were used as a target I_{Ks} for the parameter identification. A least square difference function between the simulation and experimental data was used as the cost function. The parameters of the model (Table 2) were constrained to have the same sign with respect to the initial guess. The absolute values of the parameters were constrained to be bigger than a small number ($\sim 10^{-10}$).

The I-V traces were used as a target to obtain a set of parameters which fitted more accurately to the experimental data. Only the I_{Ks} traces corresponding to test potential from 0 to 60 mV was used for the identification. This parameter set was used as the next initial guess. Then, a suitable weighting scheme was used to emphasise the importance of the relatively little deactivation data and physiologically more important first 500 ms of the I_{Ks} trace. 10 times more weight was given to every data point of tail current and 5 times more weight was given to the first 500 ms. This helped to achieve a better estimation of the tail currents and initial depolarizing current. The higher voltage traces were given more importance than the lower ones. The higher current traces were given weight 2. The weight of lower traces was decreased 0.1 for every 10 mV of testing potential.

Normalized single traces were used to improve the time kinetics of our estimates. The normalization was done with respect to the maximum value of current in the multiple traces. The tail current of short single trace was used for parameter identification. The longer single trace was used since the time point of 5.5 s. The weight 10 was given to the longer single trace.

The identified Control parameter set was used as initial guess in Acute DHA, Acute EPA and Chronic EPA identification. The G_{Ks} was constrained to the identified Control G_{Ks} in Acute cases. It was experimentally observed that the expression of KCNQ1 - KCNE1 was affected by PUFA(21). Thus the G_{Ks} which is mainly linked with the total number of channels was identified in the Chronic EPA case.

2.5 AP Simulations

The identified I_{Ks} models were then inserted into three human epicardial ventricular cell models – Grandi et al. (Grandi et al. 2009)(15), ten Tussher et al. (Tusscher et al. 2004)(16), O'Hara et al. (O'Hara et al., 2011)(14). The scaling factor $Q_{10} = 3$was used to the I_{Ks} Markov chain transition rates in order to scale its function from experimental temperature (295K) to the physiological temperature (310K)(61; 71–74). The model codes were obtained from the CellML(75–77) website (http://www.cellml.org). The Matlab codes were processed using CellML tools, i.e. COR(78; 79), to develop MATLAB codes capable of simulating APs.

2.6 Computing Resources

The parameter identification was carried out in the laboratory of Dipartimento di Elettronica, Informatica, Sistemistica (DEIS), Cesena, Italy. A cluster of 12 PCs (each with a single core CPU with speed 1.87 GHz, and running Windows XP and connected to the Matlab licence server in Bologna) was used for the identification runs. A complete parameter identification run took typically 2 days. 3600 computation hours were spent to obtain the final results presented in this study for all four cases.

3 Results

3.1 I_{Ks} Model Identification Under Control Conditions

The parameter identification of the Markov chain model of the I_{Ks} channel(22) was performed to reproduce the Control current traces. All the parameters of the model and the maximal conductance G_{Ks} were optimized simultaneously using the Nelder-Mead simplex algorithm. Whole experimental traces were used to find appropriate set of parameters as in preliminary study(61). The initial guess for the Control parameter identification was the parameter set published for the human ventricle cells(22).

Further, the appropriate weighting scheme was used and the parameter identification started again with the previously identified parameter set as new initial guess. This helped to improve fitting of relatively short tail current and of the physiologically most important part - first 500 ms of the depolarizing current.

Figure 10 shows the Control case experimental data (top row) and simulation (bottom row). Experimental data are shown as average current traces. Simulated current traces visually overlapped the experimental data. Column A) shows multiple-traces protocol. However, only the current traces for most positive testing potential (0 – 60 mV) were used for fitting, the lower current traces fits appropriately.

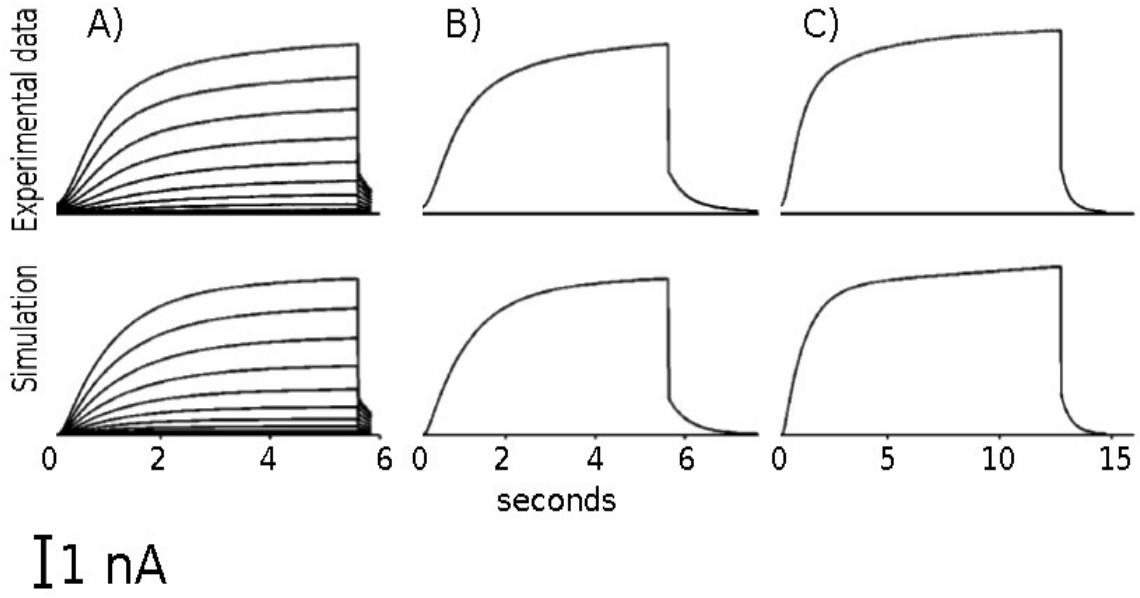

Figure 10: Control experimental data and simulation.

The first row shows the experimental data. The second row shows the simulation. Column A) shows the I-V multiple traces. Column B) shows shorter single trace. Column C) shows longer single pulse.

The short single trace shown in Figure 10 column B) was used to improve the model kinetics in deactivation. There were 2 s of tail current unlike in multiple-traces register where only 0.25 s of tail current are available.

The long single traces shown in Figure 10 column C) was used to reveal the slow kinetics of the I_{Ks} channel in 12.5 s long depolarizing pulse. The second part of the depolarizing current in the 12.5 s long depolarizing pulse (from 5.5 s to 12.5 s) gave unique information which was not unveiled by the shorter protocols. The weighting scheme was used to give more importance to this part of depolarizing current. Table 4 (on the page *26*) shows the identified set of parameters.

3.2 I_{Ks} Model Identification Under Acute DHA Conditions

The parameter identification of the Markov chain model of the I_{Ks} channel(22) was performed to reproduce the Acute DHA experimental traces. All the parameters of the model were identified simultaneously using the Nelder-Mead simplex algorithm. Whole experimental traces were used to find appropriate set of parameters as in preliminary study(61).

The number of I_{Ks} channel was not altered by the Acute exposure to DHA. The maximal conductance G_{Ks} is mainly linked to the number of I_{Ks} channels. Thus the G_{Ks} was fixed to same value as identified in the Control case.

The identified Control parameter set was used as the initial guess for the parameter identification. With this initial guess the algorithm was not able to identify appropriate set of parameters. Further the parameter set was manually changed to obtain initial guess which reproduced better the currents kinetics. With this the identified

parameter set was improved.

Finally, the appropriate weighting scheme was used, and the parameter identification started again with the previously identified parameter set as new initial guess. This helped to improve fitting of relatively short tail current, and of the physiologically most important part - first 500 ms of the depolarizing current. Table 4 (on the page *26*) shows the identified set of parameters.

Figure 11 shows the Acute DHA current traces. The experimental data are shown as average current traces in the top row. The simulation is shown in the bottom row. The simulated current traces fits appropriately to the experimental data. Column A) shows multiple-traces protocol. However, only the current traces for most positive testing potential (0 – 60 mV) were used for fitting, the lower current traces fits appropriately.

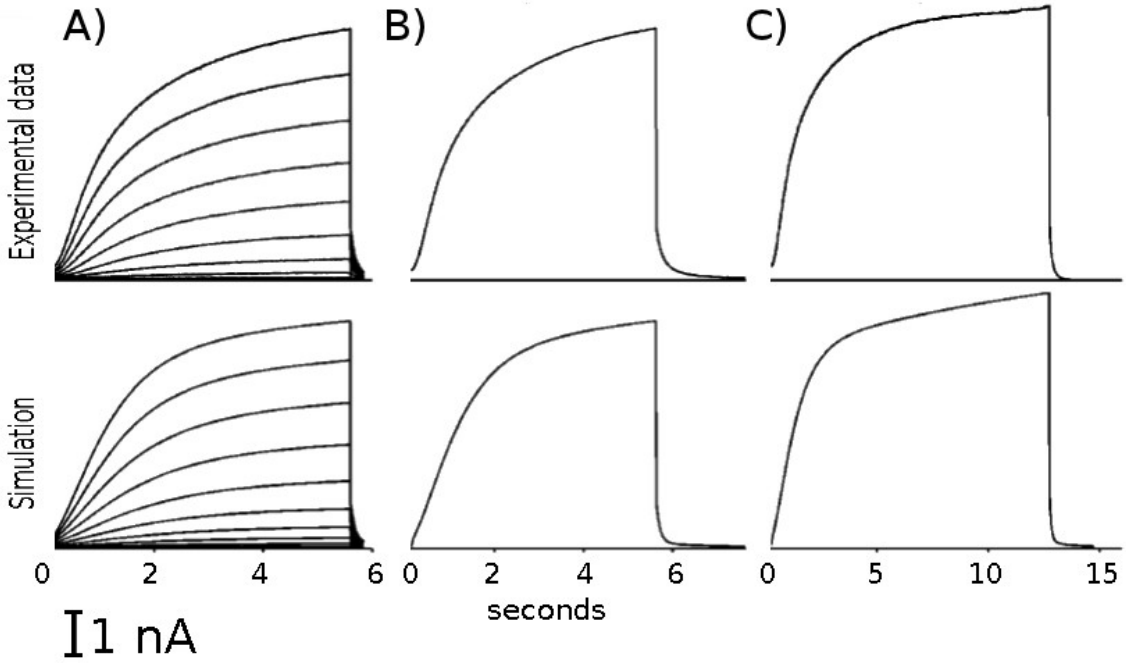

Figure 11: Acute DHA experimental data and simulation.

The first row shows the experimental data. The second row shows the simulation. Column A) shows the I-V traces. Column B) shows 5.5 s long single depolarizing trace. Column C) shows 12.5 s long depolarizing pulse.

The short single trace shown in Figure 11 column B) was used for improve the model kinetics in deactivation. There are 2 s of tail current unlike in multiple-traces register where only 0.25 s of tail current are available.

The long single trace Figure 11 column C) was used to reveal the slow kinetics of the I_{Ks} channel in 12.5 s long depolarizing pulse. The second part of the depolarizing current in the 12.5 s long depolarizing pulse (from 5.5 s to 12.5 s) gave unique information which was not unveiled by the shorter protocols. The weighting scheme was used to give more importance to this part of depolarizing current.

The maximum currents in Acute DHA experiments were increased with respect to the Control traces. The activation kinetics was slower. The steady-state current failed to

show saturation even in the long depolarizing pulse (12.5 s) at testing potential of +60 mV. The deactivation was faster than in Control.

3.3 I_{Ks} Model Identification Under Acute EPA Conditions

The parameter identification of the Markov chain model of the I_{Ks} channel(22) was performed to reproduce the Acute EPA experimental traces. All the parameters of the model were identified simultaneously using the Nelder-Mead simplex algorithm. Whole experimental traces were used to find appropriate set of parameters as in preliminary study(61).

The number of I_{Ks} channel was not altered by the Acute exposure to EPA. The maximal conductance G_{Ks} is mainly linked to the number of I_{Ks} channels. Thus the G_{Ks} was fixed to same value as identified in the Control case.

The identified Control parameter set was used as the initial guess for the parameter identification. With this initial guess the algorithm was not able to identify appropriate set of parameters. Further the parameter set was manually changed to obtain initial guess which reproduced better the currents kinetics. With this the identified parameter set was improved.

Finally, the appropriate weighting scheme was used, and the parameter identification started again with the previously identified parameter set as new initial guess. This helped to improve fitting of relatively short tail current, and of the physiologically most important part - first 500 ms of the depolarizing current. Table 4 (on the page *26*) shows the identified set of parameters.

Figure 12 shows the Acute EPA current traces. The experimental data are shown as average current traces in the top row. The simulation is shown in the bottom row. The simulated current traces fits appropriately to the experimental data. Column A) shows multiple-traces protocol. However, only the current traces for most positive testing potential (0 – 60 mV) were used for fitting, the lower current traces fits appropriately.

The short single trace shown in Figure 12 column B) was used for improve the model kinetics in deactivation. There are 2 s of tail current unlike in multiple-traces register where only 0.25 s of tail current are available.

The long single trace Figure 12 column C) was used to reveal the slow kinetics of the I_{Ks} channel in 12.5 s long depolarizing pulse. The second part of the depolarizing current in the 12.5 s long depolarizing pulse (from 5.5 s to 12.5 s) gave unique information which was not unveiled by the shorter protocols. The weighting scheme was used to give more importance to this part of depolarizing current.

The maximum currents in Acute EPA experiments were increased with respect to the Control traces. The activation kinetics was slower. The steady-state current failed to show saturation even in the long depolarizing pulse (12.5 s) at testing potential of +60 mV. The deactivation was faster than in Control.

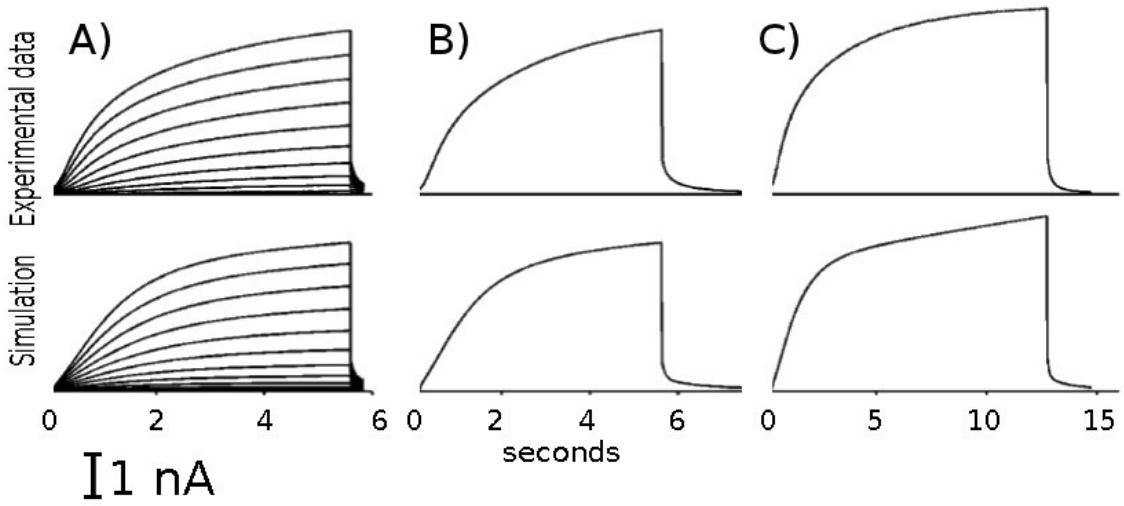

Figure 12: Acute EPA experimental data and simulation.

The first row shows the experimental data. The second row shows the simulation. Column A) shows the I-V traces. Column B) shows 5.5 s long single depolarizing trace. Column C) shows 12.5 s long depolarizing pulse.

3.4 I_{Ks} Model Identification Under Chronic 48-Hours Lasting EPA Conditions

The Markov chain model of the I_{Ks} channel(22) optimization was performed to reproduce the Chronic EPA current traces. All the parameters of the model and the maximal conductance G_{Ks} were optimized simultaneously using the Nelder-Mead simplex algorithm. Whole experimental traces were used to find appropriate set of parameters as in preliminary study(61).

The identified Control parameter set was used as the initial guess for the parameter identification. The chronic application of PUFA decreases the expression of KCNQ1(21). Thus the G_{Ks} was identified from experimental traces. Further the appropriate weighting scheme was used and the parameter identification started again with the previously identified parameter set as new initial guess. This helped to improve fitting of relatively short tail current and of the physiologically most important part - first 500 ms of the depolarizing current. Unlike the Acute cases no manual tuning of the parameters was needed to obtain satisfying parameter set.

Figure 13 shows the Chronic EPA current traces. The experimental data are shown as average current traces in the top row. The simulation is shown in the bottom row. The simulated current traces fits appropriately to the experimental data. Column A) shows multiple-traces protocol. However, only the current traces for most positive testing potential (0 – 60 mV) were used for fitting, the lower current traces fits appropriately.

The short single trace shown in Figure 13 column B) was used for improve the model kinetics in deactivation. There are 2 s of tail current unlike in multiple-traces register where only 0.25 s of tail current are available. The 12.5 s single trace was not available for the Chronic EPA case.

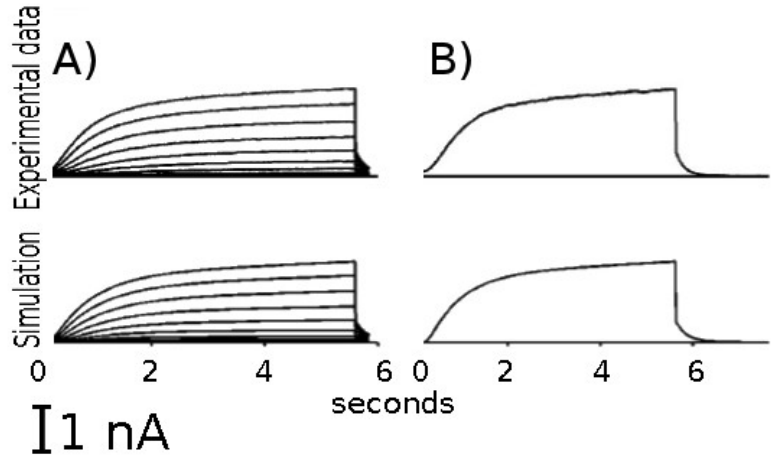

Figure 13: Chronic EPA experimental data and simulation.

The first row shows the experimental data. The second row shows the simulation. Column A) shows the I-V traces. Column B) shows short depolarizing pulse.

The maximal current was decreased with respect to Control. The depolarizing current kinetics was comparable with the Control case. The repolarization was faster than in Control. The identified G_{Ks} decreased about 20% with respect to Control G_{Ks}. The result which is consistent with the experimental observation. Table 4 (on the page 26) shows the identified set of parameters.

3.5 Model Based Analysis of I_{Ks} Gating Properties

The I_{Ks} channel simulation was performed using the I_{Ks} Markov chain model(22). The parameters were constrained to have the same sign as in the published model. All the parameters of the model were optimized. The model parameters were identified as described in previous chapters. The experimental recordings can not be simulated by the parameters published previous simulation studies(4; 22; 61). The identified parameter set based gave consistent results. The identified model parameters are shown in Table 4.

With the contribution of these parameters are described the gating properties of the model. The mathematical equation of the transition rates are shown in Table 2 on the page 12. In the chapter 1.3 is detailed description of the model. Figure 14 shows the transition rates of the model in all cases.

	Silva, Rudy parameters	Control	Acute DHA	Acute EPA	Chronic EPA
$\mathbf{m_1}$	$3.98\cdot10^{-4}$	$1.97\cdot10^{-5}$	$6.12\cdot10^{-5}$	$3.53\cdot10^{-5}$	$3.04\cdot10^{-5}$
$\mathbf{p_1}$	0.36	$7.57\cdot10^{-7}$	$6.53\cdot10^{-7}$	$1.00\cdot10^{-8}$	$6.33\cdot10^{-7}$
$\mathbf{m_2}$	$5.74\cdot10^{-5}$	$5.35\cdot10^{-6}$	$8.31\cdot10^{-6}$	$1.50\cdot10^{-5}$	$1.04\cdot10^{-5}$
$\mathbf{p_2}$	$-9.23\cdot10^{-2}$	$-1.00\cdot10^{-8}$	-0.11	$-3.80\cdot10^{-2}$	$-4.37\cdot10^{-7}$
$\mathbf{m_3}$	$3.41\cdot10^{-3}$	$2.29\cdot10^{-3}$	$7.62\cdot10^{-4}$	$7.95\cdot10^{-4}$	$2.14\cdot10^{-3}$
$\mathbf{p_3}$	0.87	0.40	0.40	0.40	0.71
$\mathbf{m_4}$	$1.20\cdot10^{-3}$	$2.91\cdot10^{-3}$	$3.88\cdot10^{-4}$	$2.93\cdot10^{-4}$	$1.70\cdot10^{-3}$
$\mathbf{p_4}$	-0.33	$-3.98\cdot10^{-3}$	$-7.58\cdot10^{-8}$	$-6.13\cdot10^{-6}$	$-6.37\cdot10^{-6}$
$\mathbf{m_5}$	$6.47\cdot10^{-3}$	$6.03\cdot10^{-3}$	$2.13\cdot10^{-2}$	$1.34\cdot10^{-2}$	$1.86\cdot10^{-3}$
$\mathbf{m_6}$	$1.25\cdot10^{-2}$	$4.91\cdot10^{-3}$	0.12	$6.62\cdot10^{-2}$	$2.71\cdot10^{-3}$
$\mathbf{p_5}$	-0.48	-0.53	-0.83	-0.87	-0.67
$\mathbf{m_7}$	$6.33\cdot10^{-3}$	$8.47\cdot10^{-2}$	$4.93\cdot10^{-2}$	$7.72\cdot10^{-2}$	$6.95\cdot10^{-2}$
$\mathbf{p_6}$	1.27	$4.82\cdot10^{-6}$	$3.52\cdot10^{-2}$	$1.67\cdot10^{-4}$	$1.16\cdot10^{-8}$
$\mathbf{m_8}$	$4.91\cdot10^{-3}$	$3.23\cdot10^{-2}$	$1.15\cdot10^{-2}$	$9.98\cdot10^{-3}$	$7.20\cdot10^{-2}$
$\mathbf{p_7}$	-0.68	$-2.12\cdot10^{-8}$	$-1.10\cdot10^{-7}$	$-5.10\cdot10^{-7}$	$-1.00\cdot10^{-8}$
$\mathbf{G_{Ks}}$	79.80	65.00	65.00	65.00	43.00

Table 4: Identified parameters for Control, and all PUFA cases.

Parameters p_i are in ms^{-1}. Parameters m_i have arbitrary units. G_{Ks} is in nS. In the first column are shown the Silva and Rudy parameters. This parameters were used as the initial guess for the parameter identification in the Control case. The second column shows identified set of parameters in Control case. This set of parameters was used as the initial guess in the parameter identification of the rest of the cases. Identified parameter set for Acute DHA is shown in third column. Identified parameter set for Acute EPA is shown in column four. Identified parameter set for Chronic EPA is shown in the last column.

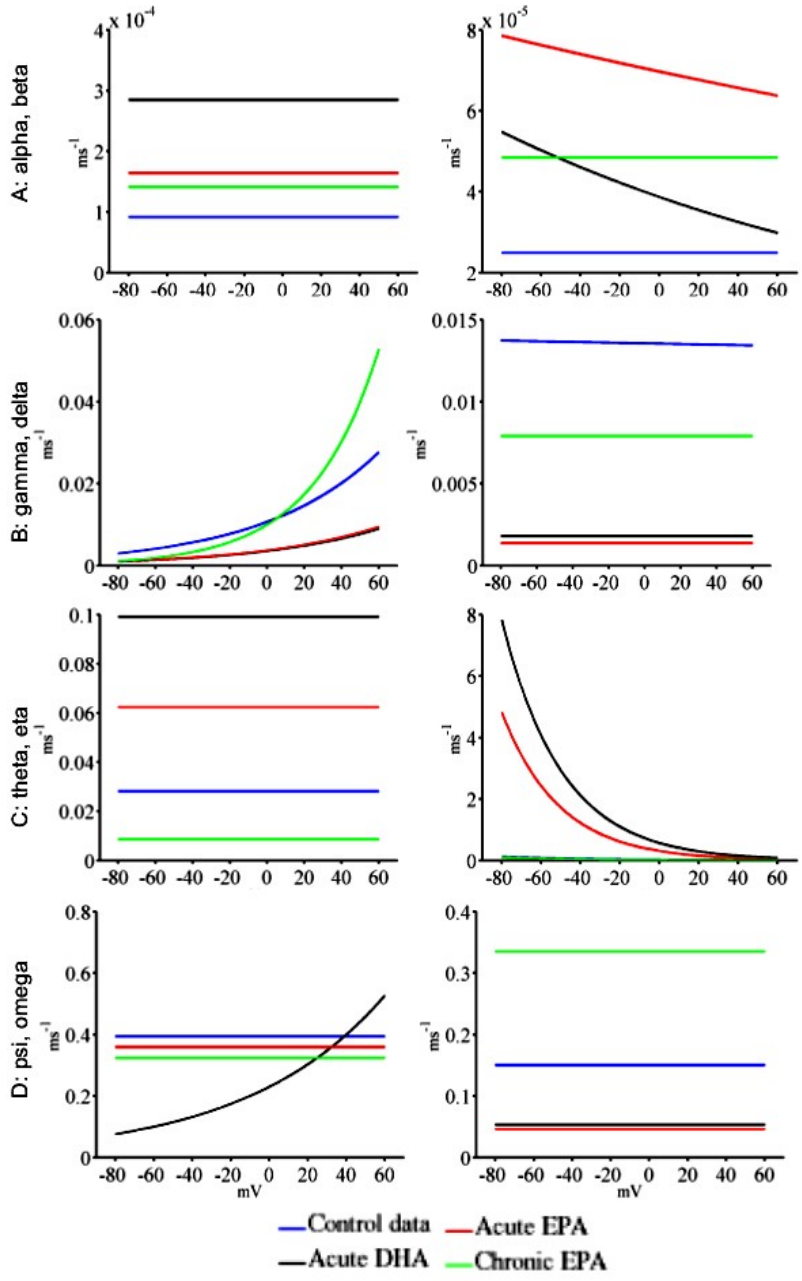

Figure 14: Transition rates of the 17 states Markovian model.

Row A shows α (left) and β (right). Row B shows γ (left) and δ (right). Row C shows θ (left) and η (right). Row D shows ψ (left) and ω (right). Blue line denotes original Control data transition rates. Black line denotes Acute DHA transition rates. Red lines denote Acute EPA transition rates. Green lines denote Chronic EPA transition rates. The same colour scheme is used in all panels.

It should be noted that transition rates in both Acute cases and in Control and Chronic cases shows similar features as seen in β, γ, δ, ω. Interestingly the parameters α, δ and ω seems to be approximately voltage-independent in all cases as was previously described only for θ(80). The voltage-independency is also evident in Control and Chronic

β and Ψ transition rates.

Figure 15 describe the dynamic evolution of model state occupancy during both single traces protocols. The model state occupancy is defined as the ratio between the number of channel in a state and total number of channels. Zone 2 kinetics was slower than in the previous studies due to reduced transition rates α and β. During the depolarization the channel moves rapidly from the Zone 1 states to the open states. The channel in Zone 2 moves slowly to the Zone 1.

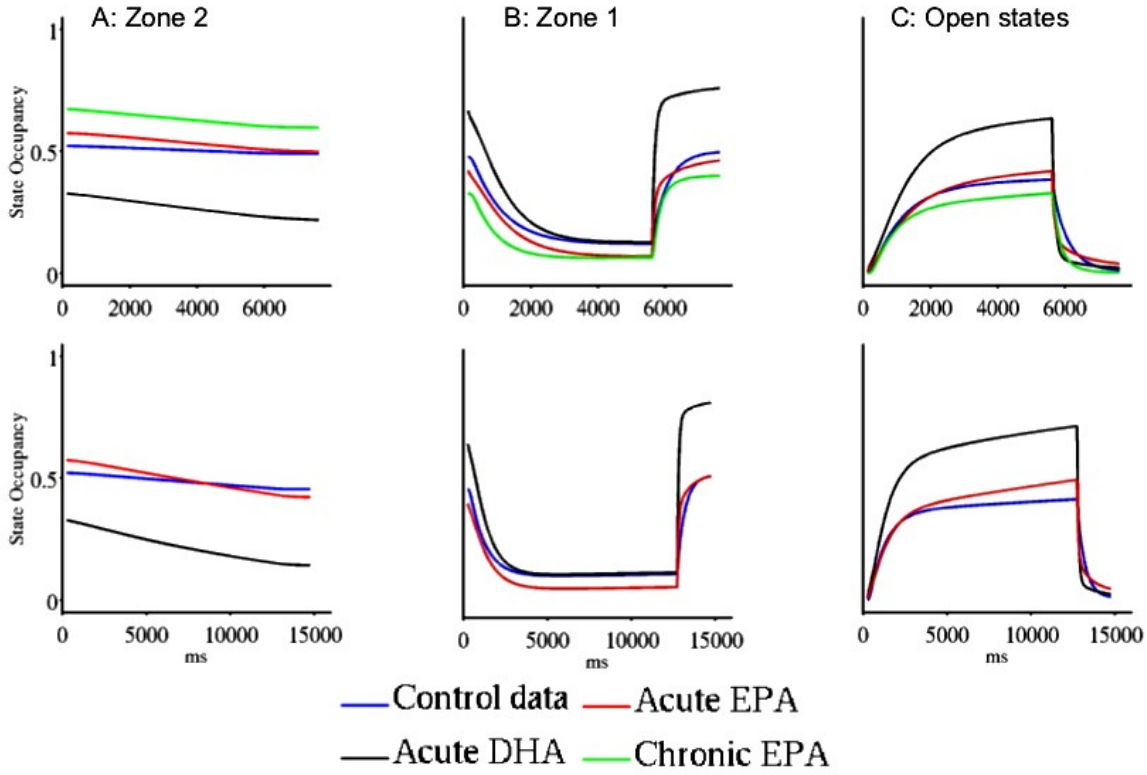

Figure 15: Markov chain state occupancy in single traces.

The top row shows the 5.5 s depolarizing trace. The bottom row shows 12.5 s depolarizing trace. Column A shows the Zone 2 (deep close) states occupancy. Column B shows Zone 1 (superficially closed) states occupancy. Blue lines denotes Control data. Black lines denotes Acute DHA. Red lines denote Acute EPA. Green lines denote Chronic EPA. The same colour scheme is used in all panels.

The effects of PUFAs were analysed in the steady-state condition. The I_{Ks} model was held on potentials from -80 to 60 mV in steps of 20 mV for 1000 s. This allowed the stabilization of the model. Then the state occupancy was calculated for Zone 2, Zone 1 and Open states. The results are shown in Figure 16.

In the potential of -80 mV all the channels resided in closed states. Up to the potential of -40 mV the states-occupancies were minimally affected. The Zone 1 remained almost unchanged till 0 mV, while the Zone 2 occupancy decreased and Open-state occupancy increased. At higher potentials the Open-state occupancy increased while Zone 1 and Zone 2 states-occupancies kept decreasing. At the potential of 60 mV the majority of the channel resided in the Open-state and only minimally in the Zone 2 states.

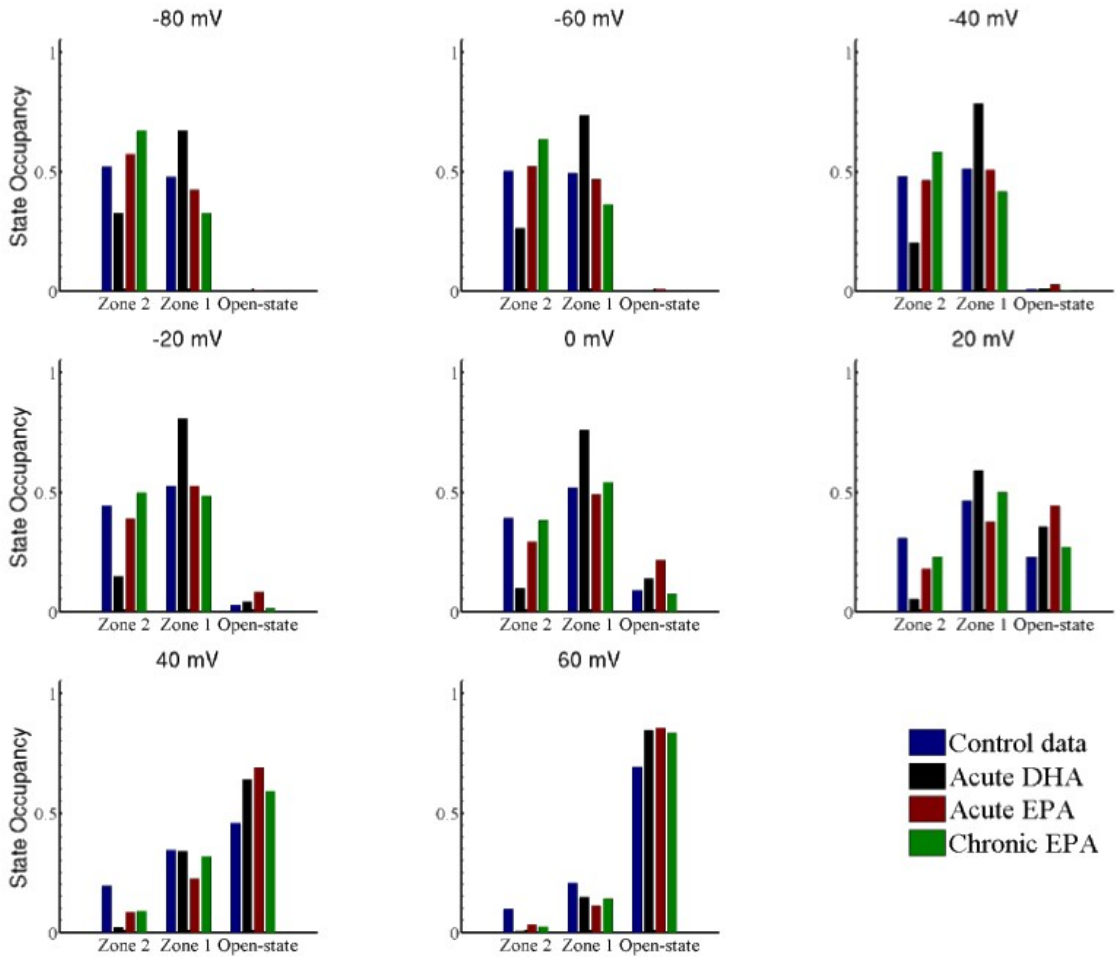

Figure 16: Steady-state distribution of model states occupancy at selected voltages.

The voltage is in the title in each panel. Zone 2 represent the deep closed states. Zone 1 represent the states close to Open-state. State occupancy is the ratio between number of channels in the state and total number of channel. Blue bar denotes Control data, black bar denotes Acute DHA. Red bar denotes Acute EPA and green bar denotes Chronic EPA in all panels.

As compared to the single trace occupancy Figure 15. In Control and both EPA cases more than 50% of channels resided in deep closed states. This is visible also after 5.5 s of depolarizing pulse to the test potential of +60 mV. The transition from the Zone 2 has very slow kinetics causing big closed states reserve. The accumulation of channels residing in Zone 2 explain the fact that even after 12.5 s depolarizing pulse the experiments failed to show clear-cut saturation as observed in majority of the cases.

Figure 17 shows the steady-state states-occupancies. As in previous model-based experiment the steady-state was simulated at each holding potential for a duration of 1000 s. The model was held on potential ranging from -80 mV to 60 mV in steps of 2.5 mV.

The Zone 2 occupancy monotonically decreased with the increasing potentials. While at potential of -80 mV more than 50% of the channels resided in Zone 2 in majority of the cases, at potential of 60 mV the number of channels in Zone 2 was minimal. Acute

DHA showed the lowest Zone 2 occupancy.

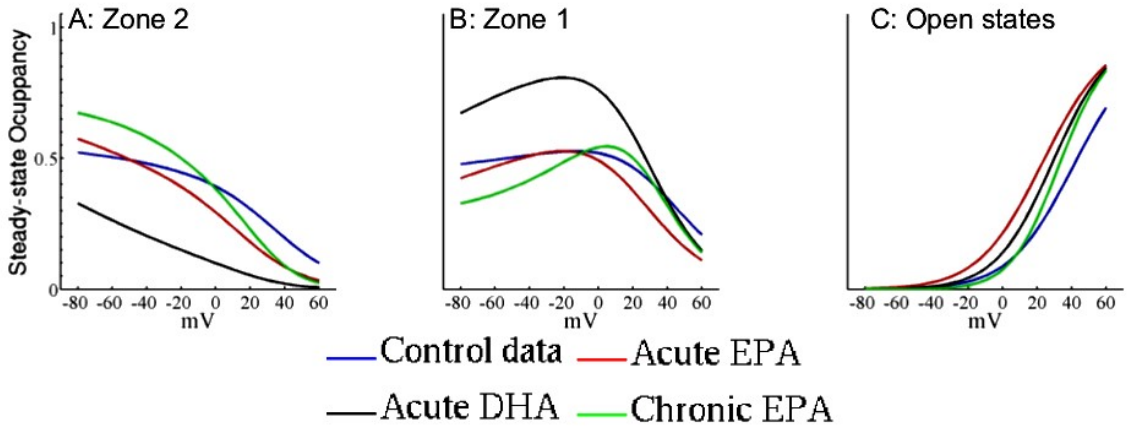

Figure 17: Steady-state Markov chain states occupancy.

Panel A shows Zone 2 occupancy. Panel B shows Zone 1 occupancy. Panel C shows Open states occupancy. Blue lines denotes Control data. Black line denotes Acute DHA. Red lines denotes Acute EPA. Green lines denotes Chronic EPA case. The same colour scheme is used in all panels. Steady state was simulated for 1000 s for each potential. State occupancy is the ratio between number of channel in the state and total number of channels.

The evolution of steady-state occupancy in Zone 1 was not monotonic. The maximum of Zone 1 occupancy was at -20 mV in Control, Acute DHA and Acute EPA cases and at 5 mV at Chronic DHA. The Acute DHA showed the highest Zone 1 occupancy compared to the other cases. The occupancy of the other cases resided about 40% at the potential of -80 mV and at the potential of 60 mV it was about 15%.

The Open-states occupancy had monotonically increasing tendency. The gain of function of I_{Ks} due to PUFA is apparent from the increased Open-state occupancy in all PUFA cases.

3.6 Simulation of Altered AP Due to I_{Ks} Changes: Effects of PUFA

The effects of PUFA on human ventricle AP and I_{Ks} was analysed based on computational cell models. Three human ventricle epicardial cell models were used – Grandi et al.(15), ten Tussher et al.(16), O'Hara et al.(14). The Markov chain model was implemented with the appropriate parameter set for each case. Figure 18 shows AP simulation and I_{Ks}.

The characteristic features of AP were analysed on the 11th AP and I_{Ks} profile. When no stimulus is applied than the cell potential tends to equilibrate with the resting membrane potential (RMP). The overshoot correspond to the maximal value of AP. The amplitude of AP is the sum of RMP and overshoot. The APD_{90} is defined as the time duration of AP since the beginning of depolarization until the potential is repolarized 90% of AP amplitude. The APD_{50} is defined as the time duration of AP since the beginning of depolarization until the potential polarize back 50% of AP amplitude. The maximal speed of the depolarization is calculated as maximum of the derivation dV/dt. This correspond to the maximum slope of AP.

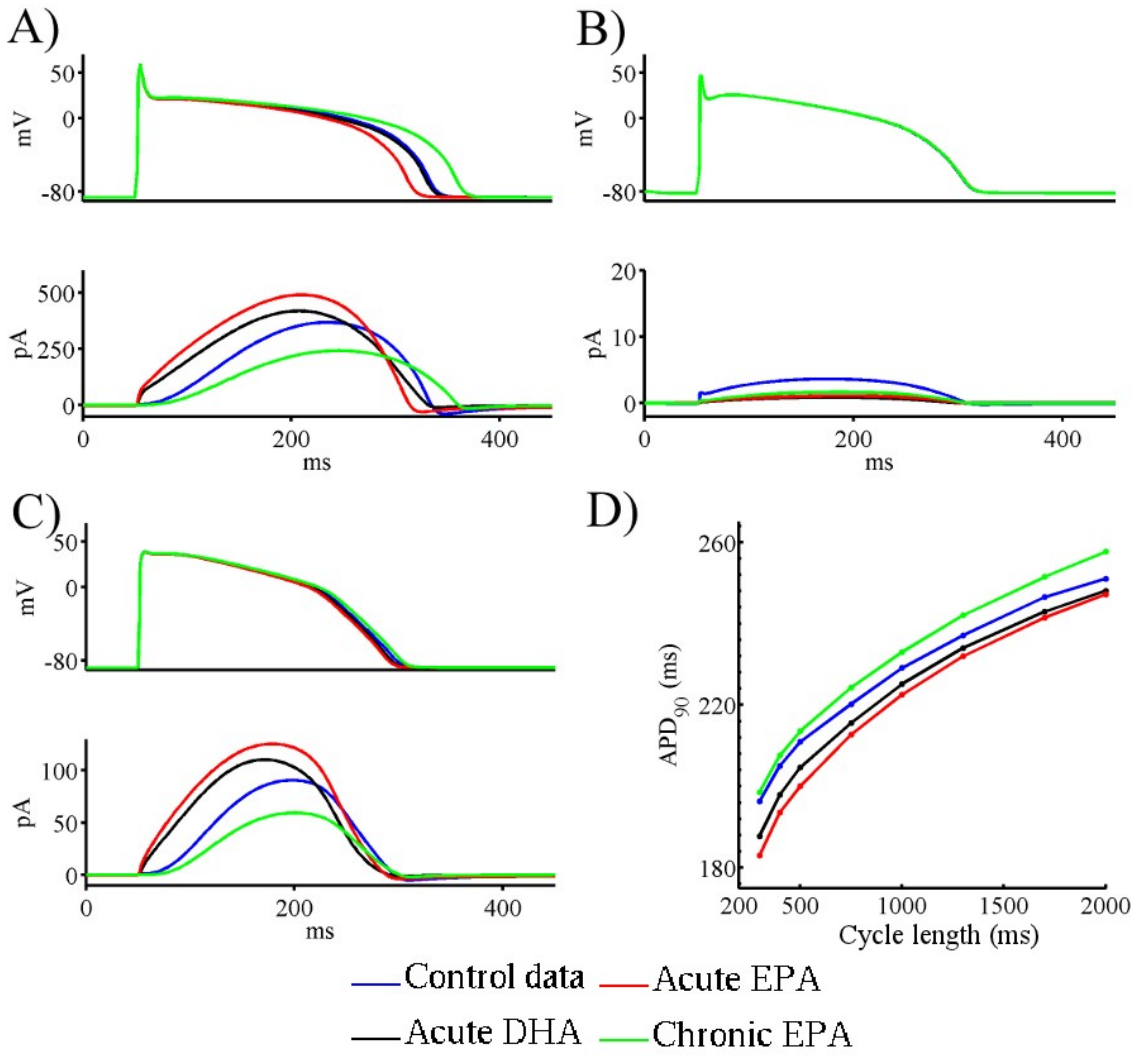

Figure 18: AP simulation results and model restitution.

Panels A, B and C shows simulated 11th APs (top chart) and I_{Ks} (bottom chart). A) ten Tusscher et al. B) Grandi et al. C) O'Hara et al. Panel D) shows the O'Hara et al. model restitution for cycle length (CL) ranging from 300 to 2000. To allow complete stabilization of the model, the simulation was performed for 300 impulses. Blue line denotes control Markov chain model. Black line denotes Acute DHA. Red line denotes Acute EPA. Green line denotes Chronic EPA.

Q_{10} scaling factor was used in order to scale the I_{Ks} from the experimental temperature (295 K) to the physiological temperature (310 K). The literature suggested Q_{10} ranging from 2 to 5(71–74). Finally, the $Q_{10} = 3$ was chosen as in previous I_{Ks} study(61). The identified G_{Ks} in MC was scaled to reproduce the basal model AP profiles. The same G_{Ks} was used to simulate Acute and Chronic AP.

Ventricle epicardial cell AP simulation were done with implementation of Control, Acute DHA, Acute EPA and Chronic EPA identified parameters and then compared. AP was simulated with initial condition from basal model at cycle length (CL) 1 s. The MC initial condition were simulated as steady-state condition at membrane potential -80mV.

The measurements of AP features were done on 11th AP. This allowed complete stabilization of the model.

Figure 18 panel A shows AP and I_{Ks} simulation with ten Tussher et al. model(16). The I_{Ks} is the major repolarizing current in this model. The absolute difference between longest and shortest APD was 50 ms. The Acute EPA increased the I_{Ks} and cause APD shortening. The Acute DHA increased slightly the I_{Ks} and caused insignificant APD shortening. The Chronic EPA decreased the I_{Ks} and caused APD prolongation. The Action PUFA caused the kinetics acceleration while in Control and Chronic case the onset had slower kinetic. The modelled RMP, overshoot and dV/dt was not influenced by the PUFA. In Table 5 are the characteristic feature of AP and the maximum I_{Ks}.

	APD_{90} (ms)	**APD_{50} (ms)**	**RMP (mV)**	**Overshoot (mV)**	**dV/dt max (mV/ms)**	**I_{Ks} max (pA)**
Control	282.19	235.08	-86.36	59.63	347.26	367.84
Acute DHA	279.36	229.15	-86.36	59.55	347.15	418.97
Acute EPA	261.48	214.82	-86.36	59.44	346.90	490.55
Chronic EPA	308.13	257.75	-86.36	59.75	347.50	242.40

Table 5: AP characteristic features and maximal I_{Ks} - ten Tusscher et al. model.

Figure 18 panel B shows AP and I_{Ks} simulation with the Grandi et al. model(15). The total amount of the I_{Ks} in this model is two orders lower than in ten Tusscher et al. model. For this reason the model was not sensitive to the PUFA induced I_{Ks} changes. In Table 6 are shown the characteristic feature of AP elicited by this model.

APD_{90} (ms)	**APD_{50} (ms)**	**RMP (mV)**	**Overshoot (mV)**	**dV/dt max (mV/ms)**
252.63	204.95	-80.98	46.85	459.80

Table 6: AP characteristic feature - Grandi et al. model.

The last model where the I_{Ks} was included was the O'Hara et al. model(14). This model offered compromise in the amount of I_{Ks} between ten Tusscher et al. model and Grandi et al.. The I_{Ks} current was ten times lower than I_{Kr} in this model. The results of the simulation with the O'Hara et al. model were shown in Figure 18 panel C. Table 7 shows the characteristic features of AP and maximum I_{Ks}.

The I_{Ks} seem to be equally increased in the O'Hara et al. model as in ten Tusscher et al. model. Both acute cases increased I_{Ks} current and caused APD shortening. Interestingly, the Acute DHA has not cause significant change in APD in the ten Tusscher et al. model. The Chronic EPA decreased I_{Ks} and caused APD prolongation. The Action PUFA caused the kinetics acceleration while in Control and Chronic case the onset had slower kinetic. The RMP, overshoot and dV/dt is not influenced by the PUFA in the model.

	APD_{90} (ms)	APD_{50} (ms)	RMP (mV)	Overshoot (mV)	dV/dt max (mV/ms)	I_{Ks} max (pA)
Control	241.87	196.87	-87.98	38.67	192.27	90.63
Acute DHA	237.01	194.01	-87.97	38.47	191.99	110.33
Acute EPA	234.20	191.20	-87.97	38.34	191.81	125.34
Chronic EPA	246.62	201.62	-87.97	38.65	192.28	59.30

Table 7: AP characteristic features and maximal I_{Ks} - O'Hara et al. model.

Figure 18 panel D shows APD_{90} restitution in O'Hara et al. model. CL was ranging from 300 to 2000 ms in variable step. The simulation was performed for 300 impulses. This allowed complete stabilization of the model.

The APD_{90} was shorten in faster pacing frequency (shorter CL) in all cases. The Control APD_{90} was very similar to Chronic APD_{90} at CL = 300 ms while at CL = 2 s the Control APD_{90} was closer to Acute EPA and Acute DHA APD_{90}. The Acute cases had the same APD_{90} at slower pacing frequency CL = 2 s

4 Conclusions

The presented study results described I_{Ks} gating properties in kidney-derivated cell line of African green monkey transfected with human gene coding KCNE1 - KCNQ1 protein which is known as I_{Ks} channel. The PUFA induced modulation to the I_{Ks} channel and simulation of effects on human ventricle cell AP were described in this study.

The presented study results showed that the effects of PUFA on the human I_{Ks} vary depending on the exposure duration. Effects of PUFA were reproduced by the model. Acute action of PUFA augment I_{Ks} and was a factor reducing APD. Chronic action had contrary effect due to slowing down the expression of the KCNE1 - KCNQ1.

The acute action slowed down the I_{Ks} kinetics in depolarization and speed up the inactivation kinetics. Chronic EPA does not caused significant kinetics change. The total amount of I_{Ks} current in Chronic EPA case was decreased.

Cardiac cell models predicted 2% AP shortening in both ten Tusscher at al. model and O'Hara et al. model due to Acute DHA induced modulation of I_{Ks}. Ten Tusscher et al. model predicted 3% AP shortening and O'Hara et al. model predicted 8% AP shortening due to Acute EPA induced modulation of I_{Ks}. Ten Tussher at al. model predicted 8% AP prolongation and O'Hara et al. model predicted 2% AP prolongation due to Chronic EPA induced modulation of I_{Ks}.

The O'Hara et al. model predicted 22% increase, 39% increase and 35% decrease of I_{Ks} amplitude in Acute DHA, Acute EPA and Chronic EPA case respectively. The ten Tusscher model predicted 14% increase, 33% increase and 35% decrease in Acute DHA, Acute EPA and Chronic EPA case respectively.

Results were consistent with previous studies which suggested pro-arrhythmic as

well as antiarrhythmic consequences. Thus, the impact of fish oil to each patient may depend on specific pathophysiological setting.

The results confirm that the full complexity of I_{Ks} kinetics can be simulated by the Markovian model proposed by Silva and Rudy(22). The appropriate set of parameters was identified for each experimental data set. The approach of fitting to the whole experimental traces was more appropriate than the estimation by Boltzmann fitting due to absence of clear-cut saturation.

The parameter identification cost is computationally very intensive task. 3600 computation hours were spent on a 12 PC distributed cluster. Manage all necessary simulations was time demanding even with highly automated algorithm which was used for this study. Dedicated computers are required for the studies rather than distributed environment.

4.1 Study Limitations

This study has several limitations worth to notice. The identified parameters sets are not necessary unique while based on good fit. The simplex algorithm is dependent on initial guess and may lead to a local minimum. An alternative parameters sets may be identified with similar fit to experimental data.

AP results were simulating only the effects of PUFA on I_{Ks}. The computational simulation of cell electrophysiology was limited due to difficulty of validation in human ventricular cells which is not currently possible. Further the results of AP simulation were highly model-dependent due to ongoing debate about reliability of single cell measurement of I_{Ks} in human cardiomyocytes. The Grandi at al.(15) shows very small I_{Ks} while ten Tusscher at al.(16) and O'Hara et al.(14) supposed that I_{Ks} channels are disrupted during cell isolation.

4.2 Proposal of Activities

PUFA has an effect on many cardiac channels. This study investigate only the effects on I_{Ks}. The description of the electrophysiological effects of PUFA can be done only if the action on the other cardiac channels is known. The next goal should be investigate the effects on the other cardiac channels which action is modulated by PUFA. The effects on I_{Kr}, I_{Na}, I_{CaL}, I_{K1} should be studied in the first stage. The fitting could be done by the developed algorithm using Nelder-Mead simplex algorithm. Whole current traces would be used as a target function for the parameters identification.

Further, the Ca^{+2} handling which is connected with the contraction is modulated by PUFA. The excitation-contraction coupling is supposed to be changed by PUFA. The model of PUFA effects on the contraction can help to understand the beneficial effects of diet rich on fish.

The experiments done in the final stage of development of the model of PUFA induced changes to the human ventricle cells should be performed in native cells rather than cultured cells. This helps to uncover specific features which could be not present in cultured cells experiment.

The I_{Ks} channel gating properties may be influenced by compounds which are

present in the organism in physiological condition. The effect of PUFA may be altered by such compounds. The β-adrenergic modulation of I_{Ks} channel was described in previous studies(4). The incorporation of both PUFA and β-adrenergic modulation may provide clues about the real effects of PUFA on I_{Ks} channel.

The mutations of gene coding KCNQ1 (α-subunit of I_{Ks} channel) have been implicated in familial atrial fibrillation(61). Such mutations may lead to decrease of I_{Ks} and development of life-threatening arrhythmias. The investigation of effects of PUFA on mutated I_{Ks} channel may help to treat this hereditary illness.

The leak current was subtracted as a constant for each potential yet it may have specific gating properties. Further leak current gating properties should be investigated.

The algorithm for parameter identification was done as an serial programme using only one CPU core for each run. The parameter identification resulted highly time demanding task. The code improvement would speed up the process of parameter estimation. The programme parallelization and using of dedicated clusters or high performance computing (HPC) is necessary. Moreover, further algorithm for conclusive unique identification of parameters needs to be developed.

5 References

1. Saiz J, Gomis-Tena J, Monserrat M, Ferrero JM Jr, Cardona K, Chorro J. Effects of the antiarrhythmic drug dofetilide on transmural dispersion of repolarization in ventriculum. A computer modeling study. IEEE Trans Biomed Eng 2011 Jan;58(1):43-53.

2. González T, Navarro-Polanco R, Arias C, Caballero R, Moreno I, Delpón E, Tamargo J, Tamkun MM, Valenzuela C. Assembly with the Kvbeta1.3 subunit modulates drug block of hKv1.5 channels. Mol. Pharmacol 2002 Dec;62(6):1456-1463.

3. Valenzuela C, Sánchez-Chapula J, Delpón E, Elizalde A, Pérez O, Tamargo J. Imipramine blocks rapidly activating and delays slowly activating K+ current activation in guinea pig ventricular myocytes. Circ. Res 1994 Apr;74(4):687-699.

4. Severi S, Corsi C, Rocchetti M, Zaza A. Mechanisms of beta-adrenergic modulation of I(Ks) in the guinea-pig ventricle: insights from experimental and model-based analysis. Biophys. J 2009 May;96(9):3862-3872.

5. Chorro FJ, Sanchis J. Dofetilide effects on the inhibition by trains of subthreshold conditioning stimuli. Pacing Clin Electrophysiol 2004 Mar;27(3):327-332.

6. Guizy M, Arias C, David M, González T, Valenzuela C. {Omega}-3 and {omega}-6 polyunsaturated fatty acids block HERG channels. Am. J. Physiol., Cell Physiol 2005 Nov;289(5):C1251-1260.

7. Guizy M, David M, Arias C, Zhang L, Cofán M, Ruiz-Gutiérrez V, Ros E, Lillo MP, Martens JR, Valenzuela C. Modulation of the atrial specific Kv1.5 channel by the n-3 polyunsaturated fatty acid, alpha-linolenic acid. J. Mol. Cell. Cardiol 2008 Feb;44(2):323-335.

8. Den Ruijter HM, Berecki G, Opthof T, Verkerk AO, Zock PL, Coronel R. Pro- and antiarrhythmic properties of a diet rich in fish oil. Cardiovasc. Res 2007 Jan;73(2):316-325.

9. Leaf A, Xiao YF, Kang JX, Billman GE. Prevention of sudden cardiac death by n-3 polyunsaturated fatty acids. Pharmacol. Ther 2003 Jun;98(3):355-377.

10. Dujardin KS, Dumotier B, David M, Guizy M, Valenzuela C, Hondeghem LM. Ultrafast sodium channel block by dietary fish oil prevents dofetilide-induced ventricular arrhythmias in rabbit hearts. Am. J. Physiol. Heart Circ. Physiol 2008 Oct;295(4):H1414-1421.

11. Kharche S, Yu J, Lei M, Zhang H. A Mathematical Model of Action Potentials of Mouse Sinoatrial Node Cells with Molecular Bases [Internet]. Am J Physiol Heart Circ Physiol 2011 Jul;Available from: http://www.ncbi.nlm.nih.gov/pubmed/21724866

12. Hund TJ, Rudy Y. Rate dependence and regulation of action potential and calcium transient in a canine cardiac ventricular cell model. Circulation 2004 Nov;110(20):3168-3174.

13. Shannon TR, Wang F, Puglisi J, Weber C, Bers DM. A mathematical treatment of integrated Ca dynamics within the ventricular myocyte. Biophys. J 2004 Nov;87(5):3351-3371.

14. O'Hara T, Virág L, Varró A, Rudy Y. Simulation of the undiseased human cardiac ventricular action potential: model formulation and experimental validation. PLoS Comput. Biol 2011 May;7(5):e1002061.

15. Grandi E, Pasqualini FS, Bers DM. A novel computational model of the human ventricular action potential and Ca transient. J. Mol. Cell. Cardiol 2010 Jan;48(1):112-121.

16. ten Tusscher KHWJ, Noble D, Noble PJ, Panfilov AV. A model for human ventricular tissue. Am. J. Physiol. Heart Circ. Physiol 2004 Apr;286(4):H1573-1589.

17. Burr ML, Ashfield-Watt PAL, Dunstan FDJ, Fehily AM, Breay P, Ashton T, Zotos PC, Haboubi NAA, Elwood PC. Lack of benefit of dietary advice to men with angina: results of a controlled trial. Eur J Clin Nutr 2003 Feb;57(2):193-200.

18. Caygill CP, Hill MJ. Fish, n-3 fatty acids and human colorectal and breast cancer mortality. Eur. J. Cancer Prev 1995 Aug;4(4):329-332.

19. Kang JX, Leaf A. The cardiac antiarrhythmic effects of polyunsaturated fatty acid. Lipids 1996 Mar;31 Suppl:S41-44.

20. Milberg P, Frommeyer G, Kleideiter A, Fischer A, Osada N, Breithardt G, Fehr M, Eckardt L. Antiarrhythmic effects of free polyunsaturated fatty acids in an experimental model of LQT2 and LQT3 due to suppression of early

afterdepolarizations and reduction of spatial and temporal dispersion of repolarization [Internet]. Heart Rhythm 2011 Mar;Available from: http://www.ncbi.nlm.nih.gov/pubmed/21459164

21. Moreno C, Oliveras A, Kharche S, Guizy M, Comes N, Stary T, Loussouarn G, Baró I, Severi S, González T, Felipe A, Valenzuela C. Effects of ω-3 polyunsaturated fatty acids on the function,expression and traffic of Kv7.1 channels. in preparation;

22. Silva J, Rudy Y. Subunit interaction determines IKs participation in cardiac repolarization and repolarization reserve. Circulation 2005 Sep;112(10):1384-1391.

23. Nelder JA, Mead R. A simplex method for function minimization. Computer Journal 1965;7.:308-313.

24. Augustsson K, Michaud DS, Rimm EB, Leitzmann MF, Stampfer MJ, Willett WC, Giovannucci E. A prospective study of intake of fish and marine fatty acids and prostate cancer. Cancer Epidemiol. Biomarkers Prev 2003 Jan;12(1):64-67.

25. de Deckere EA. Possible beneficial effect of fish and fish n-3 polyunsaturated fatty acids in breast and colorectal cancer. Eur. J. Cancer Prev 1999 Jul;8(3):213-221.

26. Taepavarapruk P, Song C. Reductions of acetylcholine release and nerve growth factor expression are correlated with memory impairment induced by interleukin-1beta administrations: effects of omega-3 fatty acid EPA treatment. J. Neurochem 2010 Feb;112(4):1054-1064.

27. McLennan PL, Bridle TM, Abeywardena MY, Charnock JS. Comparative efficacy of n-3 and n-6 polyunsaturated fatty acids in modulating ventricular fibrillation threshold in marmoset monkeys. Am. J. Clin. Nutr 1993 Nov;58(5):666-669.

28. Albert CM, Hennekens CH, O'Donnell CJ, Ajani UA, Carey VJ, Willett WC, Ruskin JN, Manson JE. Fish consumption and risk of sudden cardiac death. JAMA 1998 Jan;279(1):23-28.

29. Leaf A. The electrophysiologic basis for the antiarrhythmic and anticonvulsant effects of n-3 polyunsaturated fatty acids: heart and brain. Lipids 2001;36 Suppl:S107-110.

30. Xiao YF, Kang JX, Morgan JP, Leaf A. Blocking effects of polyunsaturated fatty acids on Na+ channels of neonatal rat ventricular myocytes. Proc. Natl. Acad. Sci. U.S.A 1995 Nov;92(24):11000-11004.

31. Xiao YF, Wright SN, Wang GK, Morgan JP, Leaf A. Fatty acids suppress voltage-gated Na+ currents in HEK293t cells transfected with the alpha-subunit of the human cardiac Na+ channel. Proc. Natl. Acad. Sci. U.S.A 1998 Mar;95(5):2680-2685.

32. Leifert WR, McMurchie EJ, Saint DA. Inhibition of cardiac sodium currents in adult rat myocytes by n-3 polyunsaturated fatty acids. J. Physiol. (Lond.) 1999 Nov;520 Pt 3:671-679.

33. Verkerk AO, van Ginneken ACG, Berecki G, den Ruijter HM, Schumacher CA, Veldkamp MW, Baartscheer A, Casini S, Opthof T, Hovenier R, Fiolet JWT, Zock PL, Coronel R. Incorporated sarcolemmal fish oil fatty acids shorten pig ventricular action potentials. Cardiovasc. Res 2006 Jun;70(3):509-520.

34. Leifert WR, Jahangiri A, Saint DA, McMurchie EJ. Effects of dietary n-3 fatty acids on contractility, Na+ and K+ currents in a rat cardiomyocyte model of arrhythmia. J. Nutr. Biochem 2000 Aug;11(7-8):382-392.

35. Ferrier GR, Redondo I, Zhu J, Murphy MG. Differential effects of docosahexaenoic acid on contractions and L-type Ca2+ current in adult cardiac myocytes. Cardiovasc. Res 2002 Jun;54(3):601-610.

36. Xiao YF, Gomez AM, Morgan JP, Lederer WJ, Leaf A. Suppression of voltage-gated L-type Ca2+ currents by polyunsaturated fatty acids in adult and neonatal rat ventricular myocytes. Proc. Natl. Acad. Sci. U.S.A 1997 Apr;94(8):4182-4187.

37. Xiao Y-F, Morgan JP, Leaf A. Effects of polyunsaturated fatty acids on cardiac voltage-activated K(+) currents in adult ferret cardiomyocytes. Sheng Li Xue Bao 2002 Aug;54(4):271-281.

38. Doolan GK, Panchal RG, Fonnes EL, Clarke AL, Williams DA, Petrou S. Fatty acid augmentation of the cardiac slowly activating delayed rectifier current (IKs) is conferred by hminK. FASEB J 2002 Oct;16(12):1662-1664.

39. Bogdanov KY, Spurgeon HA, Vinogradova TM, Lakatta EG. Modulation of the transient outward current in adult rat ventricular myocytes by polyunsaturated fatty acids. Am. J. Physiol 1998 Feb;274(2 Pt 2):H571-579.

40. Macleod JC, Macknight AD, Rodrigo GC. The electrical and mechanical response of adult guinea pig and rat ventricular myocytes to omega3 polyunsaturated fatty acids. Eur. J. Pharmacol 1998 Sep;356(2-3):261-270.

41. Judé S, Bedut S, Roger S, Pinault M, Champeroux P, White E, Le Guennec J-Y. Peroxidation of docosahexaenoic acid is responsible for its effects on I TO and I SS in rat ventricular myocytes. Br. J. Pharmacol 2003 Jun;139(4):816-822.

42. Xiao Y-F, Ke Q, Chen Y, Morgan JP, Leaf A. Inhibitory effect of n-3 fish oil fatty acids on cardiac Na+/Ca2+ exchange currents in HEK293t cells. Biochem. Biophys. Res. Commun 2004 Aug;321(1):116-123.

43. Den Ruijter HM, Berecki G, Belterman CNW, Schumacher CA, Baartscheer A, Fiolet JWT. Fish oil reduces the number of calcium after-transients and delayed afterdepolarizations in isolated yocytes from fabbits with hearth failure. Circulation 2005;112

44. Negretti N, Perez MR, Walker D, O'Neill SC. Inhibition of sarcoplasmic reticulum function by polyunsaturated fatty acids in intact, isolated myocytes from rat ventricular muscle. J. Physiol. (Lond.) 2000 Mar;523 Pt 2:367-375.

45. Leifert WR, Dorian CL, Jahangiri A, McMurchie EJ. Dietary fish oil prevents asynchronous contractility and alters Ca(2+) handling in adult rat cardiomyocytes. J. Nutr. Biochem 2001 Jun;12(6):365-376.

46. Swan JS, Dibb K, Negretti N, O'Neill SC, Sitsapesan R. Effects of eicosapentaenoic acid on cardiac SR Ca(2+)-release and ryanodine receptor function. Cardiovasc. Res 2003 Nov;60(2):337-346.

47. O'Neill SC, Perez MR, Hammond KE, Sheader EA, Negretti N. Direct and indirect modulation of rat cardiac sarcoplasmic reticulum function by n-3 polyunsaturated fatty acids. J. Physiol. (Lond.) 2002 Jan;538(Pt 1):179-184.

48. Honen BN, Saint DA, Laver DR. Suppression of calcium sparks in rat ventricular myocytes and direct inhibition of sheep cardiac RyR channels by EPA, DHA and oleic acid. J. Membr. Biol 2003 Nov;196(2):95-103.

49. Macías A, Moreno C, Moral-Sanz J, Cogolludo A, David M, Alemanni M, Pérez-Vizcaíno F, Zaza A, Valenzuela C, González T. Celecoxib blocks cardiac Kv1.5, Kv4.3 and Kv7.1 (KCNQ1) channels: effects on cardiac action potentials. J. Mol. Cell. Cardiol 2010 Dec;49(6):984-992.

50. Alonso JM, Ferrero JM Jr, Hernández V, Moltó G, Saiz J, Trénor B. A grid computing-based approach for the acceleration of simulations in cardiology. IEEE Trans Inf Technol Biomed 2008 Mar;12(2):138-144.

51. Severi S, Pogliani D, Fantini G, Fabbrini P, Viganò MR, Galbiati E, Bonforte G, Vincenti A, Stella A, Genovesi S. Alterations of atrial electrophysiology induced by electrolyte variations: combined computational and P-wave analysis. Europace 2010 Jun;12(6):842-849.

52. Severi S, Corsi C, Cerbai E. From in vivo plasma composition to in vitro cardiac electrophysiology and in silico virtual heart: the extracellular calcium enigma. Philos Transact A Math Phys Eng Sci 2009 Jun;367(1896):2203-2223.

53. Grandi E, Pasqualini FS, Pes C, Corsi C, Zaza A, Severi S. Theoretical investigation of action potential duration dependence on extracellular Ca2+ in human cardiomyocytes. J. Mol. Cell. Cardiol 2009 Mar;46(3):332-342.

54. Ciandrini A, Severi S, Cavalcanti S, Fontanazzi F, Grandi F, Buemi M, Mura C, Bajardi P, Badiali F, Santoro A. Model-based analysis of potassium removal during hemodialysis. Artif Organs 2009 Oct;33(10):835-843.

55. HODGKIN AL, HUXLEY AF. Movement of sodium and potassium ions during nervous activity. Cold Spring Harb. Symp. Quant. Biol 1952;17:43-52.

56. A.A. Markov. Extension of the limit theorems of probability theory to a sum of variables connected in a chain. reprinted in Appendix B of: R. Howard. Dynamic Probabilistic Systems, volume 1: Markov Chains. John Wiley and Sons. 1971;

57. Silva JR, Pan H, Wu D, Nekouzadeh A, Decker KF, Cui J, Baker NA, Sept D, Rudy Y. A multiscale model linking ion-channel molecular dynamics and electrostatics to the cardiac action potential. Proc. Natl. Acad. Sci. U.S.A 2009 Jul;106(27):11102-11106.

58. Rodríguez B, Tice BM, Eason JC, Aguel F, Ferrero JM Jr, Trayanova N. Effect of acute global ischemia on the upper limit of vulnerability: a simulation study. Am. J. Physiol. Heart Circ. Physiol 2004 Jun;286(6):H2078-2088.

59. Trénor B, Romero L, Ferrero JM Jr, Sáiz J, Moltó G, Alonso JM. Vulnerability to reentry in a regionally ischemic tissue: a simulation study. Ann Biomed Eng 2007 Oct;35(10):1756-1770.

60. Ravens U, Cerbai E. Role of potassium currents in cardiac arrhythmias. Europace 2008 Oct;10(10):1133-1137.

61. Abraham RL, Yang T, Blair M, Roden DM, Darbar D. Augmented potassium current is a shared phenotype for two genetic defects associated with familial atrial fibrillation. J. Mol. Cell. Cardiol 2010 Jan;48(1):181-190.

62. Ravn LS, Aizawa Y, Pollevick GD, Hofman-Bang J, Cordeiro JM, Dixen U, Jensen G, Wu Y, Burashnikov E, Haunso S, Guerchicoff A, Hu D, Svendsen JH, Christiansen M, Antzelevitch C. Gain of function in IKs secondary to a mutation in KCNE5 associated with atrial fibrillation. Heart Rhythm 2008 Mar;5(3):427-435.

63. Imredy JP, Penniman JR, Dech SJ, Irving WD, Salata JJ. Modeling of the adrenergic response of the human IKs current (hKCNQ1/hKCNE1) stably expressed in HEK-293 cells. Am. J. Physiol. Heart Circ. Physiol 2008 Nov;295(5):H1867-1881.

64. Virág L, Iost N, Opincariu M, Szolnoky J, Szécsi J, Bogáts G, Szenohradszky P, Varró A, Papp JG. The slow component of the delayed rectifier potassium current in undiseased human ventricular myocytes. Cardiovasc. Res 2001 Mar;49(4):790-797.

65. Terrenoire C, Clancy CE, Cormier JW, Sampson KJ, Kass RS. Autonomic control of cardiac action potentials: role of potassium channel kinetics in response to sympathetic stimulation. Circ. Res 2005 Mar;96(5):e25-34.

66. Powell MJD. On Search Directions for Minimalization Algorithms. Mathematical Programming 1973;4:193-201.

67. McKinnon KIM. Convergence of the Nelder-Mead simplex method to a non-stationary point. SIAM J Optimization [date unknown];9:148-158.

68. Arias C, Guizy M, David M, Marzian S, González T, Decher N, Valenzuela C. Kvbeta1.3 reduces the degree of stereoselective bupivacaine block of Kv1.5 channels. Anesthesiology 2007 Oct;107(4):641-651.

69. González T, Longobardo M, Caballero R, Delpón E, Tamargo J, Valenzuela C. Effects of bupivacaine and a novel local anesthetic, IQB-9302, on human cardiac K+

channels. J. Pharmacol. Exp. Ther 2001 Feb;296(2):573-583.

70. ModelDB: Role of KCNQ1 and IKs in cardiac repolarization (Silva, Rudy 2005) [Internet]. [date unknown];[cited 2011 Jul 28] Available from: http://senselab.med.yale.edu/modeldb/showmodel.asp?model=55748

71. Kössler F, Lange F, Caffier G, Küchler G. External potassium and action potential propagation in rat fast and slow twitch muscles. Gen. Physiol. Biophys 1991 Oct;10(5):485-498.

72. Kiyosue T, Arita M, Muramatsu H, Spindler AJ, Noble D. Ionic mechanisms of action potential prolongation at low temperature in guinea-pig ventricular myocytes. J. Physiol. (Lond.) 1993 Aug;468:85-106.

73. Filippov V, Krishtal O. The mechanism gated by external potassium and sodium controls the resting conductance in hippocampal and cortical neurons. Neuroscience 1999;92(4):1231-1242.

74. Dilger JP, Brett RS, Poppers DM, Liu Y. The temperature dependence of some kinetic and conductance properties of acetylcholine receptor channels. Biochim. Biophys. Acta 1991 Apr;1063(2):253-258.

75. Lloyd CM, Halstead MD, Nielsen PF. CellML: its future, present and past. Prog BIophys Mol Biol. 2004 Jul;85(2-3):433-50.

76. Miller AK, Marsh J, Reeve A, Garny A, Britten R, Halstead M, Cooper J, Nickerson DP, Nielsen PF. An overview of the CellML API and its implementation. BMC Bioinformatics 2010;11:178.

77. Beard DA, Britten R, Cooling MT, Garny A, Halstead MDB, Hunter PJ, Lawson J, Lloyd CM, Marsh J, Miller A, Nickerson DP, Nielsen PMF, Nomura T, Subramanium S, Wimalaratne SM, Yu T. CellML metadata standards, associated tools and repositories. Philos Transact A Math Phys Eng Sci 2009 May;367(1895):1845-1867.

78. Garny A, Noble D, Hunter PJ, Kohl P. CELLULAR OPEN RESOURCE (COR): current status and future directions. Philos Transact A Math Phys Eng Sci 2009 May;367(1895):1885-1905.

79. Garny A, Kohl P, Noble D. CELLULAR OPEN RESOURCE (COR): a public CellML based enviroment for modelling bilogical function. Inf J Bif Chaos 2003;13(3579):3579-3590.

80. Zagotta WN, Hoshi T, Aldrich RW. Shaker potassium channel gating. III: Evaluation of kinetic models for activation. J. Gen. Physiol 1994 Feb;103(2):321-362.